

Review

# Polymer Nanocomposite Membranes

Svetlana V. Kononova <sup>1,\*</sup>, Galina N. Gubanova <sup>1</sup>, Eleonora N. Korytkova <sup>2</sup>, Denis A. Sapegin <sup>3</sup>,  
Katerina Setnickova <sup>4</sup>, Roman Petrychkovych <sup>4</sup> and Petr Uchytíl <sup>4</sup>

<sup>1</sup> Institute of Macromolecular Compounds of the RAS, Bolshoi pr. VO 31, St. Petersburg 199004, Russia; gubanovagn@yandex.ru

<sup>2</sup> Grebenshikov Institute of Silicates Chemistry of the RAS, Adm. Makarova emb., 2, St. Petersburg 199034, Russia; elkor@list.ru

<sup>3</sup> LLC S&R Systems, Kosygina pr., 23/1, 180, St. Petersburg 199034, Russia; dasapegin@sr-systems.ru

<sup>4</sup> Institute of Chemical Process Fundamentals of the CAS, Rozvojova 135, CZ-165 02 Prague, Czech Republic; setnickova@icpf.cas.cz (K.S.); petrickovic@icpf.cas.cz (R.P.); uchytíl@icpf.cas.cz (P.U.)

\* Correspondence: svetlanavkononova@gmail.com; Tel.: +7-812-328-6897

Received: 11 June 2018; Accepted: 12 July 2018; Published: 19 July 2018



**Abstract:** Based on the results of research works reflected in the scientific literature, the main examples, methods and approaches to the development of polymer inorganic nanocomposite materials for target membranes are considered. The focus is on membranes for critical technologies with improved mechanical, thermal properties that have the necessary capabilities to solve the problems of a selective pervaporation. For the purpose of directional changes in the parameters of membranes, effects on their properties of the type, amount and conditions of nanoparticle incorporation into the polymer matrix were analyzed. An influence of nanoparticles on the structural and morphological characteristics of the nanocomposite film is considered, as well as possibilities of forming transport channels for separated liquids are analyzed. Particular attention is paid to a correlation of nanocomposite structure-transport properties of membranes, whose separation characteristics are usually considered within the framework of the diffusion-sorption mechanism.

**Keywords:** polymer-inorganic nanocomposite; membrane; pervaporation

## 1. Introduction

*Nanotechnology in Polymer Science. Nanocomposites*

Nanotechnology, it is assumed, will play a greater role in the near future. In the review [1], the most exact statement was given, that nano-scale relates to the transition zone between the macro-level and the molecular level. Polymer science has always been associated with nanotechnology, as many polymer objects, functionally significant or used in practice, are nano-scale. For example, separated phases in heterogeneous polymer systems often have nanoscale dimensions, besides that, inter-polymer layers and morphological domains in polymer blends, asymmetric membranes or multilayer films in some cases have nano-sized functionally-active fragments of their structure [1]. Among the tasks of breakthrough polymer science, e.g., the tasks of fundamental importance in the coming decades—the creation of hybrid polymeric materials has been allocated by many specialists [2,3]. One reason for the great importance and prospects of this field of research is the possibility of the development of composites with new or enhanced properties as compared to the initial components [4,5]. New approaches (new sight) for the development of effective and low-cost polymer composites are needed [6].

Significant improvements in the properties of polymer systems can be a consequence of their structural and morphological changes induced by nano-fillers. Introduction of nano-fillers could

lead to the improvement of structural and morphological properties of polymer matrixes. So, the relationship between synthesis, structure and properties of nanocomposites must be established for the enhancement of mechanical parameters of new materials, such as toughness and strength [7–10].

A mechanical performance of the composite of a polymer-nano-filler type depends both on the type of filler and on the polymer matrix used. Influence of a nano-level of a composite system on a macroscopic behavior (mechanical, dynamical, dielectric and transport) is reviewed in Reference [11]. The main attempts were devoted to find the correlation between a dimension of nano-fillers, their orientation, content, or dispersibility in a matrix, and the physical-chemical properties of nanocomposites based on it. In the papers of the scientific group of authors named above, the mechanical properties of polyimide (PI) films with nanoparticles of different morphology types (plates, nanotubes and sphere) were presented. Authors concluded that PI nanocomposites filled with silicate nanotubes (SNT) and tubular vapor-grown carbon nanofibers (VGCF) nanoparticles showed an increased tensile modulus with increasing volume concentration of the nanoparticles without a catastrophic decrease in the elongation at the break. The effects of various nanoparticles introduced into polyetherimide Ultem-1000—such as carbon nanofibers, nanocones/discs, halloysite hydrosilicate nanotubes (NT), and quasi-spherical zirconia particles doped with yttrium—on the mechanical behavior of nanocomposites were performed [12]. The introduction of nanoparticles into the polymer increases the Young's moduli and yield stress of block materials relative to those of the unfilled polymeric material.

Polyimide nanocomposite films (PI-PM) prepared from the poly(amic acid) of poly(pyromellitic dianhydride-co-4,4'-oxydianiline) (PM) containing the optimized concentration of nanoparticles (montmorillonite (MMT), SNT, ZrO<sub>2</sub> particles) showed an increase in tensile modulus with increasing nanoparticle concentration in the order MMT > SNT > ZrO<sub>2</sub>. The PI-PM films containing 10 vol % of SNT and ZrO<sub>2</sub> showed higher sample failure strains, in contrast to the PI-PM/MMT films. This effect suggests that the SNT and ZrO<sub>2</sub> may be more effective in improving the ductility of the polyimide nanocomposites, when the relatively brittle polyimide-MMT films are not useable. The results confirm our expectation that the morphology of the nanoparticles (platelets, tubes or isometric form) and especially their aspect ratios strongly influences the viscoelastic properties of the nanocomposites in both their solid and liquid states. Therefore, understanding the role of the nano-filler variables such as morphology, aspect ratio and composition on the properties of polymer nanocomposites could lead to development of new materials with optimal properties for targeted application areas. It was shown that tensile strength and deformation-at-break of the PI-PM-based nanocomposite films decreased slightly with increasing concentrations of the nano-filler used to an extent that depends on the specific characteristics of the nano-filler used, in particular, on its ability to aggregate. This decrease in tensile strength may be attributed to the less than optimum adhesion between the nano-fillers and the matrix and the possible formation of an inhomogeneous network structure density in the nanocomposite. Despite the reduction of the tensile strength caused by the incorporation of the nano-fillers in the polyimide nanocomposites, authors noted that the incorporation of relatively high concentrations of SNT and ZrO<sub>2</sub> (up to 10 vol %) do not lead to a drastic decrease of elongation-at-break ( $\epsilon_t$ ) that is widely reported in the literature for a number of PI nanocomposites containing organo-clay nano-fillers [13,14]. This important benefit offered by the SNT and ZrO<sub>2</sub> was believed to be due to the desirable intrinsic properties of these particles that can be prepared with the prescribed properties for specific applications including polymer nanocomposites, as already mentioned [11,15].

It was shown that an improvement in the mechanical characteristics of the material was achieved by introducing into the polymer matrix (poly{1,3-bis(3,4-dicarboxyphenoxy)benzene [4,4-bis(4''-N-phenoxy)-diphenyl sulfone]imide} (PI P-SOD)) about 10% MMT [16]. For this purpose, the MMT has been pre-modified (aminoethylaminomethyl)phenethyltrimethoxysilane. After the filling of PI P-SOD with magnesium silicate nanoparticles modified with silane (10 wt %), the nanocomposite strength increased by 15%, bending elastic modulus and shear elastic modulus by a factor of 1.4.

Incorporation of magnesium hydrosilicate NTs in polymer films improved their mechanical properties without notable increasing of brittleness. It was shown that the average increase in the modulus value of a nanocomposite was equal 0.15 GPa per 1 wt % of incorporated NTs. Increasing in mechanical properties was observed in composites containing up to 15 wt % of magnesium NTs, simultaneously with increasing of thermo-stability. These nanocomposites possessed low dielectric constants also (~2.0) [4].

A number of other properties and potential applications are of interest including thermal stability, flammability resistance, electrical/electronic properties, barrier properties, membrane properties and others [1,2,4,11,17,18].

Normally, the addition of low-permeability fillers (such as silica) into non-porous polymer film reduces penetrant diffusion simply by volume-fraction effects [19]. The free volume decreases in these types of composites and leads to decreased molecular transport of permeate, because their molecules do not dissolve in the crystalline region of a polymer. The development of polymer membranes with inorganic crystalline fillers was considered for increasing their barrier properties with respect to gases and liquid medium [20–22]. In some cases, when nano-particles are intercalated into polymeric matrices, they are known to increase the overall mechanical strength and barrier properties [23].

Since the issue of the transport properties optimization of nanocomposite polymer membranes remains relevant to this day, there have been attempts to make some generalizations known; review papers [1,5,13,24–29]. These studies raises general questions [1,30], but in most cases the analytical generalizations were made for solving specific problems of a separation [31–36] or other tasks including fuel cells or catalytic membrane reactors applications [37–43]. In general, it is necessary to highlight review articles in which information is collected on the introduction of a certain type of nanoparticles in polymer films of different morphologies, for example membranes-containing 0D to 2D nano-fillers [37,44,45]. Much attention was paid to the effects of introducing carbon nanoparticles into the polymer matrix [46,47]. There is a lot of information about the choice of zeolite to form polymer-inorganic membranes [48–50]. It was interesting to review the search for ways of forming an optimized membrane due to filling with nanoparticles of polymers of a certain class, for example, polyimides or polysulfones [26,27,47,51–53]. Separately, we would like to mention review works aimed at developing techniques for the target formation of membranes of certain structural and morphological characteristics, notably, taking into account the existing ideas about the mechanism of selective transport of penetrants [15,29,34,36,39,47,51,54].

This publication presents an analytical review that takes into account the main aspects outlined in the above summarizing publications, but additionally, original studies that provide valuable information for understanding processes involving nanoparticle-loaded polymeric membranes. A critical analysis of the available information is directed to the identification of the most significant factors influencing the gas separation and pervaporation properties of composite membranes of this type. Particular attention is of the influence of structural and morphological characteristics on the transport properties of diffusion nanocomposite membranes on the example of composite materials containing hydrothermal magnesium silicate nanoparticles.

## 2. Polymer Nanocomposites for Membranes Applications

Recently, polymeric nanocomposite membranes have been widely used in various applications, such as gas separation, water purification, desalination, fuel cells, etc. [10,32,34,40,55,56]. Most of the currently used membranes are polymeric, and their production is highly developed [57], but they are usually not suitable for critical technologies, in particular for very high temperature applications [58]. The trade-off between flow and selectivity underlies the optimization of the diffusion membrane. Improving the functional properties of polymer membranes and developing new composite membranes by structural modification of the polymer matrix plays an important role in membrane science and technology. The modified membrane can have excellent stability in a wide range of process conditions, high selectivity for the target chemicals, and can also have a large

molecular flux of penetrants with a small driving force. Polymeric nanocomposite membranes with enhanced performances such as high selectivity, fluxes and favorable surface morphology have been prepared by incorporating nano-size fillers into a polymer matrix [59–61].

Rheology properties of solvents or melts of polymer nanocomposites were investigated [4,16]. By including nano-size fillers into the polymer solution (melt) prior to the membrane fabrication, one can change its rheology (depending on the nature of the distribution of nanoparticles in casting dispersed mixtures). This makes it possible to form membranes of a different morphology, as follows:

(i) The principle named ‘particle-assisted wetting’, based on the templating process with the introduction of nanoparticles into the acrylate-based reaction mixture, was the basis for a new method for preparing membranes with high porosity and uniform pore distribution [62–64]. A typical example of the preparation of membranes for the size-based separation is set forth below. A mixture of a hydrophobic monomer, monodisperse silica nanoparticles hydrophobized by a silanization, and a photoinitiator, formed a monolayer of particles on the water surface. After curing with UV irradiation and the subsequent removal of the particles with hydrofluoric acid, a thin porous membrane was obtained. Results of further experiments of authors [64] showed that these membranes on suitable support can be effectively used for the separation of substances in size.

(ii) Multi-walled carbon nanotubes (MWCNTs)/polysulfone blend membranes were prepared by a phase inversion process, using N-methyl-2-pyrrolidinone as a solvent and water as a coagulant. For the formation of blend membranes, MWCNTs were first treated with strong acid to make them well dispersed in organic solvents with the preparation of homogeneous MWCNTs/polysulfone dispersions. Because of the hydrophilic MWCNTs, the surface of the MWCNTs/polysulfone blend membranes appeared to be more hydrophilic than in the case of just a polysulfone membrane. The pore size of the blend membranes increased along with the contents of MWCNTs up to 1.5%, then decreased, and at 4.0% of MWCNTs it became even smaller than that of polysulfone membrane. The polysulfone membrane with 4.0% of MWCNTs showed higher flux and rejection than the polysulfone membrane without MWCNTs [65].

(iii) The organic-inorganic nanocomposites obtained on sol-gel chemistry can underlie both porous and non-porous diffusion membranes. For nanocomposite membranes based on glassy polymers with low free volume prepared by a sol-gel process in a polymer matrix, improvements in selectivity and permeability were reported [66,67]. For other cases, an increase in selectivity but a decrease in permeability [68] and vice-versa [69] were observed. In these studies, the results were related to an improvement in the solubility of the nanocomposite membrane [67], the change in chain packing and segmental mobility of the polymer and the type of alkoxide used [66]. New polyether imide hybrid films were prepared by a sol-gel process followed by thermal imidization using MTEOS and a poly(amic acid) containing ether linkages and isopropylidene groups [70]. Experiments on the penetration of small gas molecules (He, N<sub>2</sub>, O<sub>2</sub> and CO<sub>2</sub>) have shown that hybrid films with a higher silica content exhibit a higher permeability for all test gases. The hybrid films exhibited a trade-off between permeability and selectivity. An increase in the membrane permeability, depending on the concentration of silica, was accompanied by a slight reduction in selectivity (Figure 1). The highest gas permeability was found for the sample filled with 10% silica. These films have good O<sub>2</sub>/N<sub>2</sub> and CO<sub>2</sub>/N<sub>2</sub> separation properties.

(IV) The most often used methods are the formation of non-porous (the dimensions of the voids correspond to the transport channels of gases or liquids by the mechanism of sorption-diffusion) and microporous mixed matrix membranes (MMM). Mixing of molecular sieving particles with polymers for the production of MMM makes it possible to combine the excellent properties of gas separation of molecular sieving materials with the processability of polymers [71]. For example, zeolite-filled microporous MMM (Zeo TIPS) were formed using the thermally induced phase separation (TIPS) process and consisted of zeolite particles in a microporous polymer matrix [72]. Zeo TIPS membranes are designed to improve upon the performance of dense polymer membranes for gas or/and liquid separations and to approach the performance of zeolite membranes avoiding their

drawbacks. The model demonstrating the potential of these membranes in gas separation applications was presented in the paper. Modeling the structure shown in Figure 2 [72], it is complicated and outside the scope of this work. Instead, the membrane structure was modelled as a mixture from polymer, voids, and zeolite particles in a parallel arrangement. This model takes into account the loading of the zeolite, the ratio of the volume of voids to the volume of the polymer in the membrane, as well as the permeability properties inherent in each of the membrane components (Figure 3).

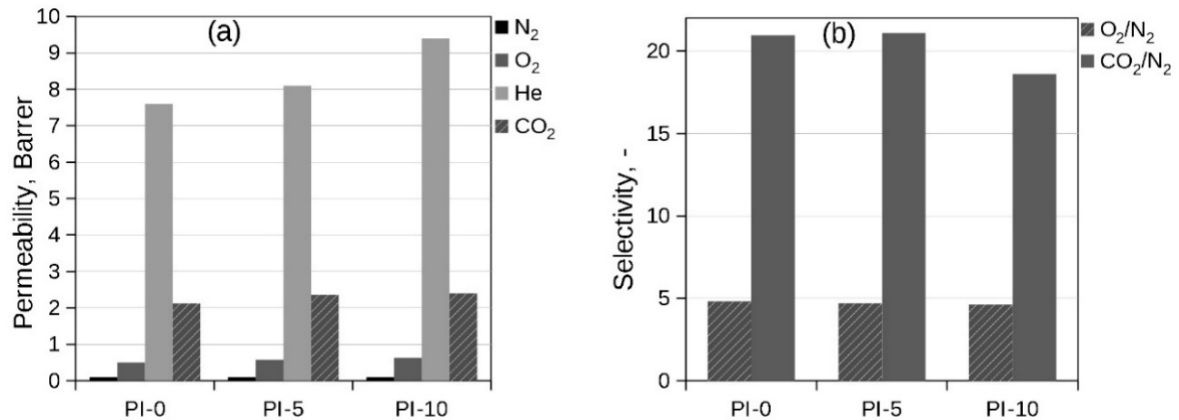


**Figure 1.** Dependence of the permeability (a) and the selectivity (b) of PI on silica content of 0% (PI-0), 5% (PI-5) and 10% (PI-10) [70].

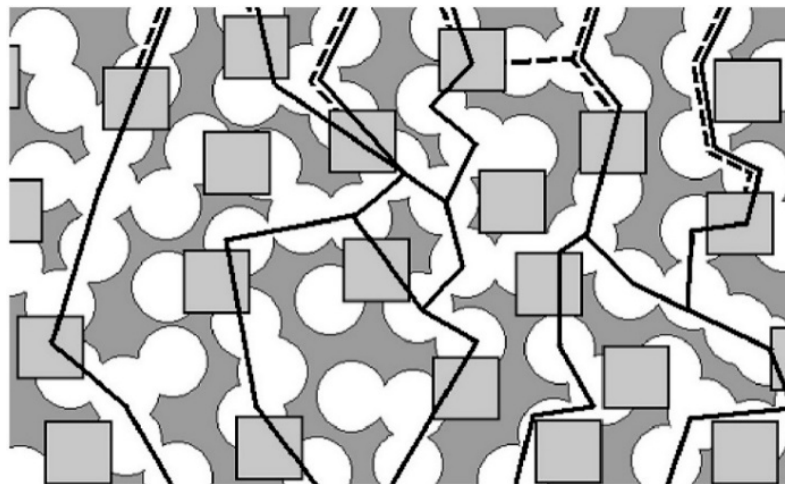


**Figure 2.** Separation schematic for the permeation of two species from the top to the bottom of the Zeo TIPS membrane. The dashed lines represent the path of the larger component. The solid lines represent the path of the smaller component [72].

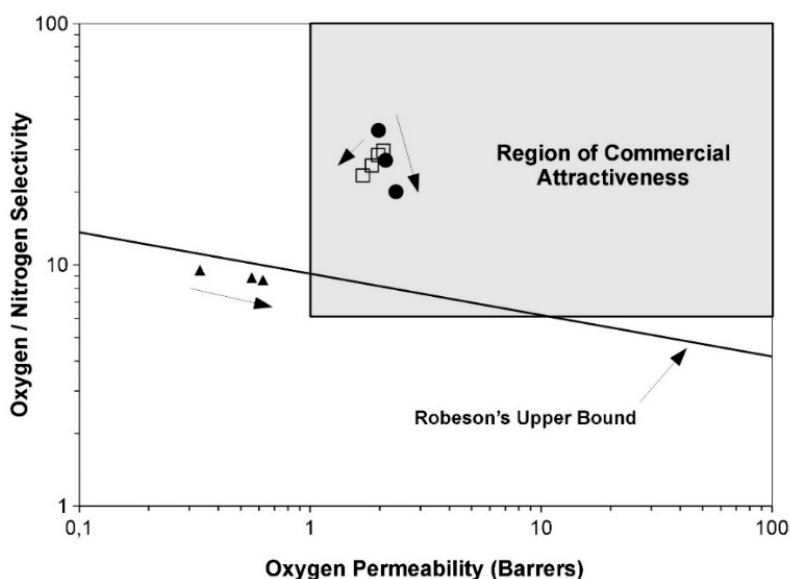


**Figure 3.** Performance of ideal Zeo TIPS membranes with an arrow indicating increasing polymer permeability (●), non-ideal Zeo TIPS membranes with an arrow indicating increasing  $\beta$  (□), and dense mixed matrix membranes (MMM) with an arrow indicating increasing polymer permeability (▲), plotted with Robeson's 1991 upper bound and region of commercial attractiveness [73]. All points correspond to 25 vol % zeolite loading and all Zeo TIPS membrane points correspond to a 3:1 ratio of void volume to polymer volume.

The correct choice of material for the matrix and sieve phases is fundamentally important for the development of the MMM [74]. The molecular sieving phase, according to the authors, should accurately distinguish the difference in size and shape of molecules. A successful example is given that a 13X zeolite with an aperture of 10 Å is unlikely to act as molecular sieves for O<sub>2</sub> and N<sub>2</sub> molecules with lengths of 3.75 and 4.07 Å, respectively, while zeolite 4A with an effective aperture size of 3.8 Å should be able to distinguish two molecules due to entropic factors [75]. Molecular sieve membranes containing zeolite or CMS possess very attractive penetration properties because of their steric, equilibrium and kinetic effects, leading to highly selective separation of molecules of similar size [76]. Both types of particles were successfully used as fillers in the formation of MMM, and their selective transport properties can be realized to varying degrees depending on the composition and method of the membrane preparation [77].

Both components contribute to the properties of the membrane, where, in the absence of defects, the selected polymer matrix corresponds to the minimum achievable characteristics, and the introduced molecular sieves contribute to improving the selectivity of the membrane [74]. Polymers with a high glass transition temperature that now dominate in gas separation membranes have high selectivity and economically acceptable permeability, which makes them successful candidates for the polymer matrix. Although the difficulties in forming a MMM using a rigid glassy polymer as a continuous phase are evident, in particular because of poor polymer contact with the polymer sieve, some success has been reached by searching for new particle introduction techniques. Good contact between the components of the membrane is necessary. Otherwise, a lower resistance to the flow of gases is possible in the interfacial region, hence, a decrease in selectivity with increasing permeability.

The great attention were attracted MMMs obtained in a result of the nanoparticles introduction in a non-porous polymer matrix. This method makes it possible to develop membranes with the improved complex of mechanical, thermo-physical properties with the maintenance of stability in the aggressive media. In Reference [78], the reason was discussed why the introduction of zeolites into a non-porous polymer matrix can really lead to an improvement in the MMM properties. In 1991, Lloyd Robeson demonstrated that there is a correlation between permeability and selectivity that

results in an upper bound for polymer membranes [79]. For actual polymer membranes, the data points would appear below a so-called “upper bound trade-off curve” [80]. This suggests that even with remarkable developments in polymer chemistry it is unlikely there will be significant changes in the permeability/selectivity trade-off in the nearest future. Newly synthesized polymeric membranes seem to obey the trade-off line between permeability and selectivity. As is known, the problem encountered by the use of the gas separation membrane is the search for a higher selectivity and permeability of the material with a high resistance to aggressive conditions. The price of the material must be competitive, and this material can easily be made into a membrane [81]. Inorganic membranes [82,83], for example, based on zeolites, may offer a solution to the permeability/selectivity trade-off problem. Their selectivity and permeability data are often in the upper right quadrant of a Robeson plot [78]. Thermally and chemically stable molecular sieve membranes with characteristics significantly exceeding the upper boundary of the interconnection curve, however, are difficult and expensive to manufacture. The development of new MMMs is considered to be the most practical approach to overcoming objective limitations in obtaining economical materials for a gas separation membrane [73,84].

An obvious strategy to bridge the gap between polymer and molecular sieve membranes is to mix them in a single composite membrane. MMMs combine the advantages of flexible, processable polymer membranes with the selectivity of inorganic membranes [25]. It would seem that to achieve membrane performance above the upper bound of a Robeson plot [78] the content of the inorganic additive should be high. Unfortunately, MMMs become brittle as the concentration of molecular sieves in the membrane increases. Typical MMM loadings are <40 wt %.

The study of MMM was mainly related to the optimization in the selection of different molecular sieves as dispersed particles in different polymers, both with high and low glass transition temperatures [77].

According to Reference [49], the first attempt to study MMM was undertaken by Paul et al. in 1973. They used zeolite 5A in silicone rubber and observed delayed diffusional time lag but found no improvement in gas separation properties [49]. The authors observed good contact between the polymer and inorganic phases, linking this effect mainly with the soft and flexible structure of the rubber-like polymer [75]. However, some researchers have shown that the advantage of including a molecular sieves phase in a highly permeable rubbery polymer is in most cases minimal, since most of the penetrant diffusion will be passing through a polymer phase that exhibits less flow resistance than the molecular sieves. For example, poly (dimethylsiloxane) (PDMS) with high O<sub>2</sub> permeability (933 barrer) and low selectivity for O<sub>2</sub>/N<sub>2</sub> (2.1) can only give a minimal gain in the transport properties of a MMM, that by characteristics is much lower than the trade-off curve [75]. Large improvement could only be observed at very high loading inorganic fractions. In this case, the mechanical properties of the membrane approach to “the difficult-to-process membrane”.

After some reports of improved separation characteristics associated with the addition of zeolites to rubber polymers, the focus of attention shifted to mixed zeolites with glassy polymers [71]. Most glassy polymers can provide commercially acceptable minimum matrix phase characteristics, as compared to a rubber polymer. As mentioned above, the initial attempts to manufacture MMM using glassy polymers and zeolites resulted in voids in the interfacial region. This reduces the characteristics of the separation of the MMM relative to the polymer in its composition [72,85]. Efforts to eliminate these non-selective sites were often focused on using binding agents to induce favorable interactions between the polymer and the zeolite, on adding a plasticizer to increase the flexibility of the polymer matrix, or on searching for ways of chemically linking two components [27,86,87]. As result of efforts to eliminate these voids, the resulting permeability of the MMM was often sacrificed.

Thus, the MMM should ideally be a homogeneous mixture of polymer and molecular sieve, but this is rarely realizable [28]. Adding a filler material such as zeolite (KA, NaA, CaA, and NaX zeolites) to the polymer membrane network was reported to improve the PVA membrane performance [88]. It was shown that in zeolite-PVA membranes the separation factor was unchanged

at low zeolite content and it decreases at high zeolite content because the more zeolite particles in the membrane, the more chances of creating a less selective leak around the zeolite particles.

Most zeolite membranes are composites with a medium pore size of 0.55 nm. It is shown that ZSM-5 in the MMM is characterized by good contact between the nanoparticles and the polymer, since the polymer chains can penetrate the mesopores of ZSM-5. The pores of ZSM-5 crystals provide size and shape selectivity. The ideal H<sub>2</sub>/CH<sub>4</sub> separation factor increased from 83.3 to 169 at 20% loading [89]. In Reference [90], new polyimide (PI) films containing zeolite L and/or silica, having a thickness of tens of micrometers, and their gas transport properties were studied with respect to the film's structure. The gas permeability (O<sub>2</sub>, N<sub>2</sub> and CO<sub>2</sub>) increased with an increase in the inorganic content in the composite film, while the selectivity was maintained constant in comparison with the PI film. For the 10% filled samples, there was not any observation of the significant enhancement in the gas transport characteristics. The results of the SEM cross section analysis of the film showed good compatibility between the polymer and the inorganic phase, and also indicated a dense membrane structure comparable to the structure of PI without nano-fillers (PI-0). The highest gas permeability was found for the sample filled with 20% of zeolite (PI-20). The permeability of N<sub>2</sub>, O<sub>2</sub>, and CO<sub>2</sub> through PI-20 film increased, compared to the reference PI film PI-0, while the selectivity for the O<sub>2</sub>/N<sub>2</sub> and CO<sub>2</sub>/N<sub>2</sub> gas pairs remained almost unchanged. Similar behavior was reported in the literature for hyperbranched PI-silica hybrid membranes, when O<sub>2</sub>/N<sub>2</sub> selectivities were maintained almost constant although their O<sub>2</sub> permeability increased with increasing silica content [91].

O<sub>2</sub>/N<sub>2</sub> and CO<sub>2</sub>/CH<sub>4</sub> selectivities of ODPA-TAPOB hyperbranched polyimide-silica hybrid membranes are discussed in [91,92]. The O<sub>2</sub>/N<sub>2</sub> selectivity depends on the diffusivity selectivity rather than the solubility selectivity. The  $\alpha$  (O<sub>2</sub>/N<sub>2</sub>) values of the hybrids were maintained almost constant although their O<sub>2</sub> permeability increased with increasing silica content. For CO<sub>2</sub>/CH<sub>4</sub> separation, noticeable enhancement of CO<sub>2</sub>/CH<sub>4</sub> selectivity was observed and the  $\alpha$  (CO<sub>2</sub>/CH<sub>4</sub>) value of the hybrids increased with increasing silica content. The ODPA-TAPOB-silica hybrid membranes demonstrated  $\alpha$  values that correspond to the  $\alpha$  values of the upper boundary Robeson's curve of the CO<sub>2</sub>/CH<sub>4</sub> separation with an increase in the silica content. According to the author, the high CO<sub>2</sub>/CH<sub>4</sub> selectivity of the membrane is due to the inclusion of silicon dioxide.

Suer et al. studied the preparation and pretreatment effect on the structure and performance of MMM [2,50]. MMMs made from polyethersulfone (PES) with hydrophilic zeolites 13X or 4A demonstrated the strong effect of the membrane preparation procedure on the permeability of the gases. The rapid solvent release followed by slow drying resulted in relaxation of the molecular package, increased homogeneity and less dense structure, hence the higher penetration. It was shown that a significant improvement in permeability properties occurred at high loads. PES-13X membrane was observed to show a better separation characteristic than PES-4A. It has been suggested that the transport mechanism cannot be explained solely by the molecular sieving effect, since 13X has much larger pores than 4A. The reason could be the appearance of a cavernous porous structure around the fillers, leading to partial incompatibility of polymer chains and zeolite crystals. Differences in cave structures between PES-13X and PES-4A are due to various interactions of the zeolite and polymer, which directly affects the permeability of the MMM.

It should be noted that studies of MMM containing zeolites as nano-fillers of polymer matrix (rubbery or glassy polymers) did not lead to unambiguous conclusions about how the presence of micro- or nano-voids at the interface between the polymer and inorganic phases affects a selective transport in composite membranes. Completely opposite results of the introduction of zeolite nanoparticles into the polymer matrix, which affected the properties of the diffusion membrane, are known. Surprising enhancement of both membrane permeability and selectivity for molecular species as penetrants was also achieved by reinforcing the polymer membrane matrix with nano-fillers [9]. Synergetic advantage of nano-scale measurements ("nanoeffect") was emphasized with respect to larger scale modification. Understanding the changes in properties, when the size of the particles (or fibers) was reduced to the level of nano-scale, is important for optimizing the resulting nanocomposite.

A successful example is that the addition of silicalite to silicone rubber increases both the permeability and selectivity of small gas molecules ( $\text{CO}_2$ ,  $\text{O}_2$ ,  $\text{H}_2$ , He) relative to the initial polymer, but decreases the permeability coefficients for large molecules (such as butane) [93].

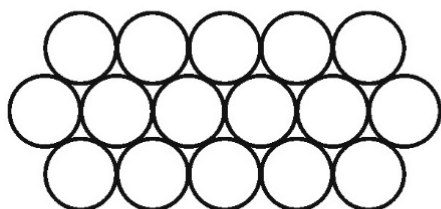
As noted above, the type of nano-filler and its own features can play a decisive role in the formation of MMM properties. Discussing the properties of MMMs above, it should be taken into account that zeolite is defined as a member of a family of hydrated alumino-silicate minerals that has a framework structure with interconnected cavities occupied by large metal cations and water molecules. The nature of these void spaces and channels determine the gas transport properties of zeolites. Zeolite molecular sieve typically has a uniform pore size within the range of 3–10 Å. Pores of zeolites completely exclude molecules that are larger than their diameter. In comparison with natural zeolites, synthetic zeolites are better suited for research and industrial applications because of their greater homogeneity in composition and purity, which can provide a high degree of reproducibility. More than 150 synthetic zeolites have been synthesized: Type A, Type X, Type Y, Type ZSM and so on. According to IZA, the structures of zeolite are MFI (ZSM-5, silicalite), IFT, AFI (aluminophosphate ALPO 4–5), LTA (Linden type A), MOR (mordenite) and FAU (faujasite) [94,95].

Many questions connected with the influence of the structural and morphological features of the MMM on the mechanism of the gaseous or liquids transport through a mixed matrix, were stated during studying zeolite-containing membranes. In spite of that, positive results were achieved for quite different objects, including membranes with nano-fillers of other types.

(V) In Reference [96] “adsorbent-filled membranes” have been tested in pervaporation for three applications: removal of organic compounds from an aqueous solution, dehydration of organic/water azeotropic mixtures, and separation of an organic/organic mixture. Authors have concluded that the potential industrial applications of these membranes depend on the properties of the adsorbents. Different types of adsorbents have been evaluated: zeolites, activated carbon, and carbon molecular sieves. Silicalite is currently considered the most promising adsorbent. It enhances, for example, the selectivity and flow through the PDMS membrane when removing organic compounds from water. The PDMS silicalite membranes can, for example, be effectively used to concentrate alcohols and aromatic compounds from dilute aqueous solutions. Adsorbent-filled membranes provide the opportunity to optimize the process of pervaporation in various applications. The conclusion was made that with the development of new microporous adsorbents, an optimization of adsorbent-filled membranes with better separation properties is expected [96].

Nano-fillers having prospects for polymer nanocomposite membrane fabrication are organic and inorganic additives, metals and metal clusters, nanoparticles, nanofibers, and mineral sheets (carbon NTs (CNTs), graphene oxide,  $\text{TiO}_2$ ,  $\text{SiO}_2$ ,  $\text{Mg}(\text{OH})_2$ ,  $\text{Al}_2\text{O}_3$ , ZnO, clay etc.) of different structure and morphology as, for example, in Figure 4.

#### Metal-Oxide Nanoparticles



#### Carbon Nanotubes

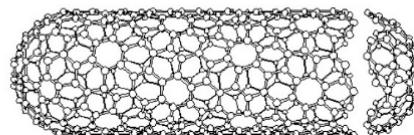
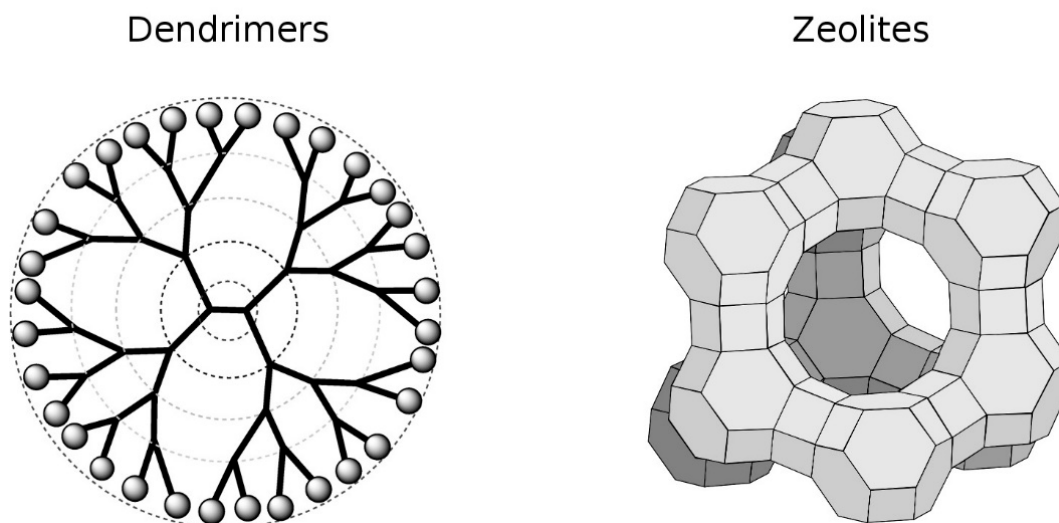


Figure 4. Cont.



**Figure 4.** Selected nanomaterials currently being evaluated as functional materials for water purification [97].

(VI) Nanoparticles themselves can form materials with interesting properties for practical use, for example, in the development of novel water-purification functional materials (e.g., nano-sorbents, redox and catalytically active nanoparticles, nanostructured membranes and bioactive nanoparticles) and processes (e.g., dendrimer enhanced ultrafiltration) [97,98].

The possibility of using CNTs as membranes for gas separation was accepted some time ago. The first verifications of this idea for single- and double-layer NTs were carried out using molecular dynamics (MD) [59]. Similar experiments were made by Hinds and co-workers with membranes from MWCNTs [99,100]. NTs were incorporated into a thin impermeable film: Holt et al. used a silicon nitride matrix, whereas Hinds et al. used polymer. The pore diameters of NTs in membranes made by Holt et al. vary from 1.3 to 2 nm, while those of NTs used by Hinds et al. lie in a much wider range. Experimental data on the permeability of single-component simple gases, in both cases demonstrate the rapid transport of penetrants. The penetration rate observed by Holt et al. for a number of gases, is one or two orders of magnitude greater than could be predicted, according to the Knudsen model [59,101]. Nanoparticles have been self-assembled, followed then by crosslinking reactions at liquid interfaces so that ultrathin membranes arose. The interstitial space between these nanoparticles should enable size-selective separations [97,102].

Carbon black reinforcement of elastomers, modification of polymers by colloidal silicon dioxide and even reinforcement with natural fibers (for example, asbestos fibers of nano-sized diameters) are typical examples of the formation of polymeric nanocomposites of practical significance. Nano-clays, have been used as effective nano-fillers for the polymer nanocomposites [17,103,104].

With the use of montmorillonite ( $\text{Na}^+\text{MMT}$ ) clay, belonging to the class of smectite clays (i.e., family of phyllosilicates 2:1), much effort has been made to use them as a filler for the development of new polymer-inorganic materials [105,106]. Smectite clays are characterized by their properties as cation exchange and intercalation of molecules, and  $\text{Na}^+\text{MMT}$  will tend to swell in some polar solvent [23].

(VII) Works with layered nano-materials were associated, first of all, with the search for ways of creating polymer-inorganic composites with improved barrier characteristics. Much attention was paid to processes of the exfoliation of clay nanoparticles in a polymer matrix (Figure 5). Two structural types were possible when  $\text{Na}^+\text{MMT}$  was involved in the PVA matrix. The first is an intercalated structure in which one or two elongated polymer chains are inserted into the interlayer spaces of the layered clay, and the second one is the exfoliated structure in which clay layers are dispersed in the PVA matrix. In any case, the clay fillers provide a stable layer based on polymer [107].

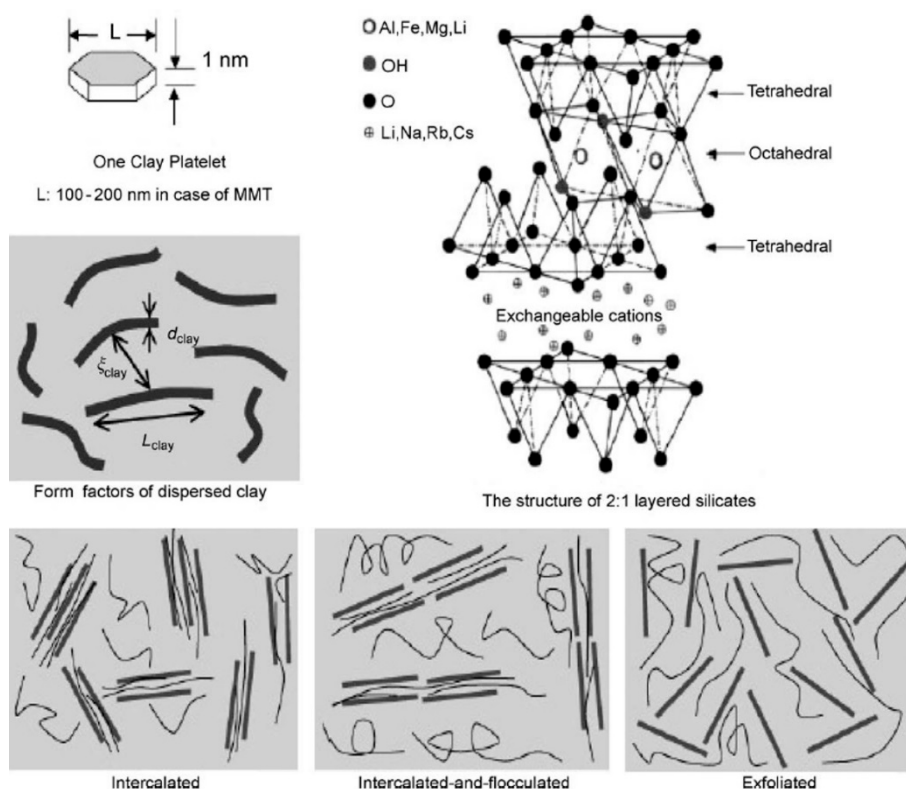


**Figure 5.** Schematic diagram showing the structure of 2:1 phyllosilicate and the polymer clay nanocomposites [13].

PDMS/MMT nanocomposites were obtained, in particular, by ultrasonic vibration, a mixture of silanol-terminated PDMS and a commercial organosilicate. Results of a WAXD study of nanocomposites detected the formation of exfoliated structures [13].

Figure 6a–d from Reference [108] are schematic diagrams illustrating a formation process of an exfoliated structure in the MMT-PA6 nanocomposite using the clay slurry. The clay slurry is first pumped under vigorous shear (Figure 6a). The slurry droplets tend to become finer during mixing (Figure 6a). Water of the slurry drops begin to evaporate on contact with molten PA6 (Figure 6b,c). During water evaporation, some silicate layers are fixed into molten PA6 and dispersed at the monolayer, and some dispersed as few stacking layers (Figure 6d). The tensile and flexural modulus as well as tensile strength of the nanocomposite containing 1.6 wt % MMT are higher than those of unfilled PA6 but the impact strength is 12% lower compared to PA6 [108].

Yano et al. have successfully used the technique for the preparation of polyimide/MMT nanocomposites from solution dimethylacetamide (DMAC), a poly (amic acid), and a DMAC dispersion of MMT modified with dodecylammonium cations [109]. In the case of 12CH<sub>3</sub>-MMT, the MMT appears to be homogeneously dispersed and the average diameter of the dispersed MMT particles was the smallest of all. The carbon number of the surfactant increases, the hydrophilicity of particles decreases WAXD patterns of the nanocomposite containing 12CH<sub>3</sub>-MMT showed almost exfoliated structure, while WAXD patterns of composites prepared with 12COOH-MMT or C10A-MMT indicated the inhomogeneous dispersion of a part of MMT in the PI matrix [109].

In another report [110], PI/MMT nanocomposites were prepared by a cast method from solutions of poly(amic acid) precursors and dodecyl-MMT in *N*-methyl-2-pyrrolidone as a solvent. The cured films of the rigid-rod PI/MMT were characterized by FTIR, TEM and WAXD as nanocomposites, being exfoliated at low MMT content and partially exfoliated at high MMT content. This method was discussed also as suitable for the preparation of nanocomposites of a type of covalently bonded layered silicate in PI.

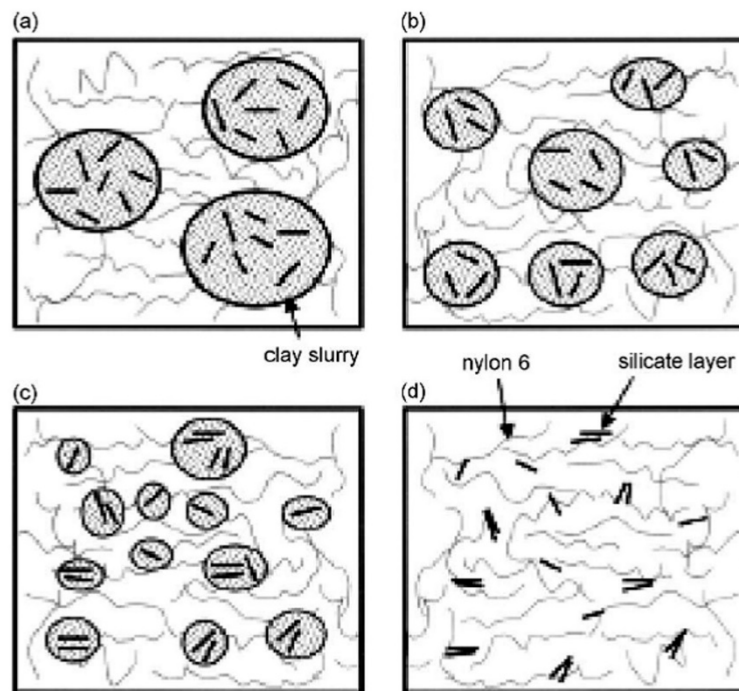


**Figure 6.** (a–d) Schematic diagrams showing dispersion of the Na-MMT silicate layers of the slurry into PA6 during compounding [108].

It was shown that the introduction of MMT into the matrix of glassy polymers could lead to a decrease in the permeability of the MMM with respect to both gases and liquids [18,111,112].

Polystyrene (PS)/clay hybrid systems have been prepared via in situ polymerization of styrene in the presence of (1) unmodified Na-MMT clay; (2) MMT modified with zwitter-ionic cationic surfactant octadecyldimethyl betaine ( $C_{18}DMB$ ) and (3) MMT modified with polymerizable cationic surfactant vinylbenzyltrimethylammonium chloride (VDAC) [113]. For all composites, an accurately proportional decrease in the permeability and diffusion of oxygen with the addition of clay was noted. The effect of clay on the oxygen solubility was significantly less. Solubility data changes were declared being within the range of experimental error of 10% with the addition of clay. These facts are demonstrated in Figure 7, presenting a plot of relative oxygen permeability  $P_c/P_0$  versus relative oxygen diffusivity  $D_c/D_0$ , where  $P_c$  and  $D_c$  are the permeability and the diffusivity of the filled polymer, and  $P_0$  and  $D_0$  are the permeability and the diffusivity of PS.

The assumption was made about the invariance of the internal solubility of the matrix  $S_0$  in the presence of mineral layers. Therefore, the polymer/clay composite solubility  $S_c$  can be expressed as  $S_c = S_0 (1 - \phi_m)$ , where  $\phi_m$  is the volume fraction of mineral phase. The authors suggested that changes in the solubility of oxygen in composites were comparable, since composites containing no more than 10% of the mineral phase were studied. The nanocomposites PS/VDAC-MMT and PS/ $C_{18}DMB$ -MMT showed significantly lower relative permeability (diffusion) comparing with the PS/Na-MMT composite containing untreated clay in the case of samples with a similar clay content. In about 3% wt/wt of clay, only 4% decrease of oxygen permeability was found by authors in the case of PS/VDAC-MMT, 8% in the case of PS/ $C_{18}DMB$ -MMT, and for PS/Na-MMT, changes of permeability were negligible. With about 9% wt/wt of clay, 18% decrease of oxygen permeability was found, 42% for PS/ $C_{18}DMB$ MMT, and only about 2% for PS/Na-MMT conventional composite.

Different continuum models have been discussed to predict the permeability of plates-filled composites. Many nanocomposite systems presented in the literature can be described using models of this type, wherein only the shape and volume of the filler fraction are required to predict the properties [1]. These models usually consider random placement (random only in two

directions) parallel plates arranged perpendicularly to the direction of penetration of substances. In Reference [114], the orientation factor was introduced. The prediction of a significant decrease in permeability of nanocomposites was given for cases of the use of fillers with a high aspect ratio. Transport properties of polymers can be significantly altered due to changes in the diffusion pathway of penetrant molecules by introducing inorganic plates with a sufficient aspect ratio [1,106].

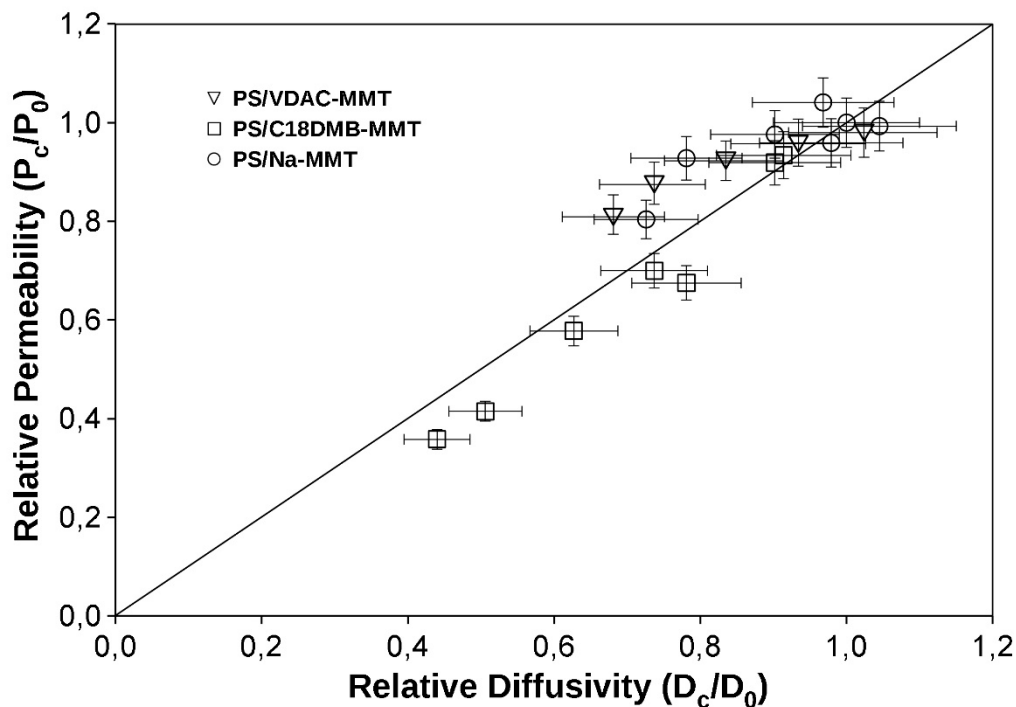


**Figure 7.** Relationship between relative permeability  $P_c/P_0$  and relative diffusivity  $D_c/D_0$  plotted for all studied composite materials [113].

Although composites based on nanoparticles are often subject to the predictions of continuum mechanics, there are situations when nanocomposites can exhibit properties being not expect for the filling with larger particles [1].

In the case of polymers loaded with plate-like inorganic fillers, including clays, semi-empirical models proposed by Nielsen [115] and by Cussler [116,117] are used to describe the gas barrier [1]. Three model PS/clay hybrid systems presented above (Figure 7) with very different layer morphologies were considered. Nazarenco et al. made a comparative analysis of the simulations of Nielsen and Cussler [113].

It was demonstrated that Nielsen's formula is more applicable to composite materials filled by discs located at a distance greater than the radius of disk  $R$  (the dilute mode) [1]. In contrast, Cussler's equation is more convenient for materials containing disks placed at a distance that are comparable to  $R$  or being less (the semi-dilute mode) [1,113,118]. At the semi-dilute mode, the volume fraction of disks  $\phi_m$  is much smaller than unity. According to Paul et al. [1], a semi-dilute mode is easier to realize using disks with a large aspect ratio  $\alpha$ . In both models, uniformly dispersed disks are arranging to orient parallel to the film surface and perpendicular to the direction of the gas molecules penetration. The models had an experimental basis, since in practice, the arrangement of the particles described above (alignment of the plates in the flow) is carried out during the formation of composites.

It is important that the basis for this prediction was the assumption that the particles had no influence on the gas solubility and the gas-diffusion characteristics of the polymer matrix.

A sketch of Nielsen's model is demonstrated in Figure 8. The main idea of the model was to evaluate the variation in the path length of the scattering molecules, taking into account both the needs to bypass obstacles (low permeability inorganic plates).

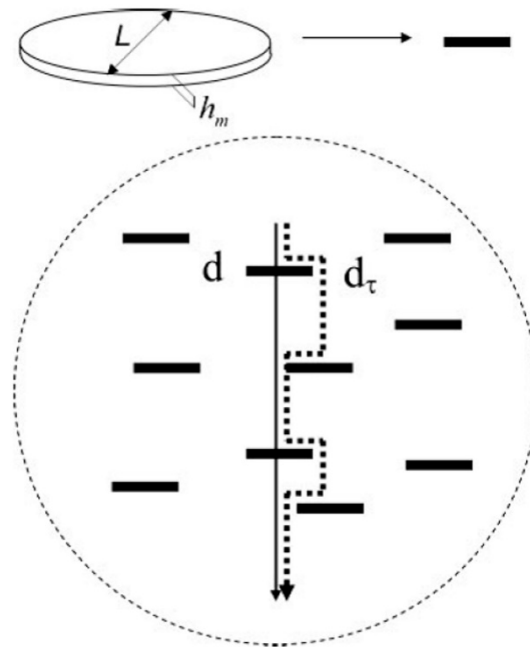


**Figure 8.** Sketch illustrating the Nielsen tortuosity diffusion model for the nanocomposite structure consisting of oriented layers (disks) homogeneously dispersed in the polymer matrix [113].

Nielsen proposed an equation for relative permeability  $P_C/P_0 = (A_c/A_0)/\tau$ , where  $A_c/A_0$  was the reduced cross section, and  $\tau$  was the maximum tortuosity factor defined as a ratio of the length of the maximum tortuous path to the length of the direct path, that is  $\tau = d_\tau/d$ .  $\tau$  can be explained as  $1 + \phi_m \alpha/2$ , where the disk aspect ratio  $a = 2R/h_m$  (see Figure 8). The reduced cross section  $A_c/A_0$  was estimated via the Delesse principle used in stereological analysis [119]. The final form of the Nielsen equation follows:

$$P_C/P_0 = \frac{1 - \phi_m}{1 - \frac{\alpha}{2}\phi_m} \quad (1)$$

The authors [113] proposed extending Nielsen's equation to take into account the random orientation of the disks in the material, and to use for this purpose a multiplied factor  $1/3$ , as was done in Reference [114,118].

$$\text{In this case, } P_C/P_0 = \frac{1 - \phi_m}{1 + 1/3(\frac{\alpha}{2}\phi_m)} \quad (2)$$

Cussler proposed the equation for the diffusion of gases in systems under discussion, that was transformed by Nazareno et al. taking into account additive contribution to solubility from the soluble polymer matrix and insoluble disk phase, into

$$P_C/P_0 = \frac{1 - \phi_m}{1 + \frac{(\phi_m \alpha/2)^2}{1 - \phi_m}} \quad (3)$$

Accenting the importance of taking into account the repeated multiple scattering of the penetrant between close pairs of disks, that is, the special physical meaning of the Cussler's equation, the authors of Reference [113] proposed the simplified morphological model and based on them simplified transport model. A sketch of this model is shown in Figure 9.

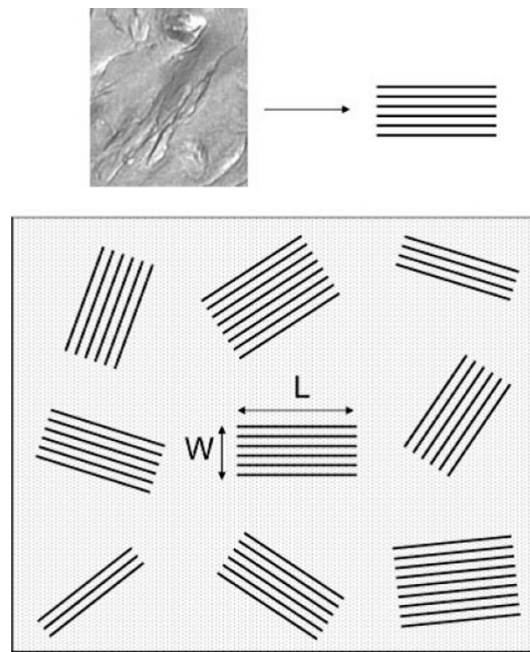


**Figure 9.** Morphological model of PS/VDAC-MMT nanocomposite system [113].

The mineral phase was represented by discs with a diameter  $2R = L = \bar{L} = 240$  nm. The discs were arranged in perfect stacks of disc's layers (aggregates). The number of layers in aggregates varied between three and nine. The interlayer distance was constant  $L = \bar{L} = 5$  nm. The disk thickness was  $h_m = 1$  nm. The stacks were homogeneously dispersed in the polymer matrix, and they were randomly oriented. It was the ideal example of a structural model for a perfect intercalated system. The transport model is essentially a modification of the original Nielsen model pictorially shown in Figure 10, wherein layers of individual particles were replaced by layers of stacks.

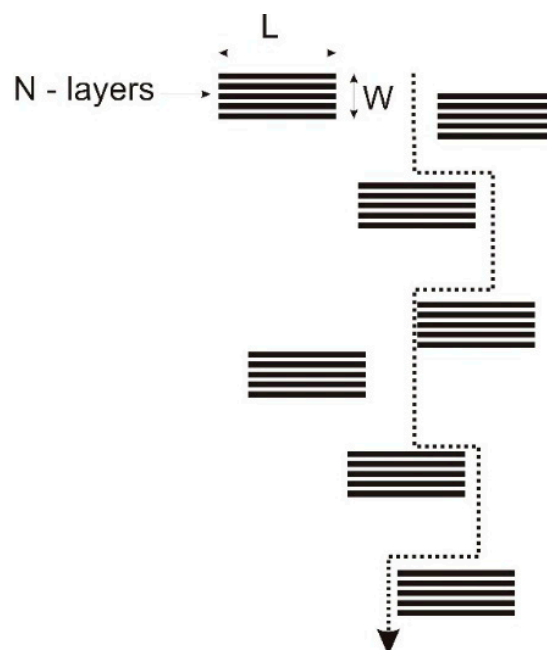


**Figure 10.** The sketch illustrating the Nielsen tortuosity model modified for the nanocomposite structure consisting of oriented layer stacks homogeneously dispersed in the polymer matrix [113].

Unlike the morphological model, the number of layers in one stack (aggregate)  $N$  was assumed to be the same for all aggregates, to simplify the analysis. The paper demonstrates good agreement between the calculation results of the gas barrier characteristics using the proposed transport model with all its assumptions and experimental data, for example, for the PS/VDAC-MMT nanocomposite.

The most interesting cases were the formation of composite MMT-containing membranes with improved selective transport properties. The water separation factor, as shown in Reference [120] can significantly increase in comparison with an unfilled PVA membrane, while the composite membrane have a reasonable flux. For the membrane type of this paper,  $\text{Na}^+$ MMT particles hardly form a continuous phase, but are isolated and surrounded by PVA chains in the matrix. According to the authors, in the mixed matrix membrane based on PVA, the mobility of the predominantly penetrating component (water) of the separated mixture can increase due to the effects associated with the introduced clay particles. These same effects contribute to a decrease in the mobility of the less permeable component (isopropanol or 1,4-dioxane).

According to experimental data, it is possible to obtain layered crystal structures in the PVA matrix due to strong intercalation when clay particles are included in the matrix [120]. The crystalline and hydrophilic nature of  $\text{Na}^+$ MMT particles was shown to hinder the transport of organic components of the mixed aqueous media to provide an easy passage of water molecules through the MMM (Figures 11 and 12). As the water content of the feed mixture increased, flux also increased due to hydrophilic-hydrophilic interactions. In addition to the increased plasticization effect of the PVA membrane in the presence of a large amount of water during the transport process, the separation factor has decreased due to a decrease in crystallinity.

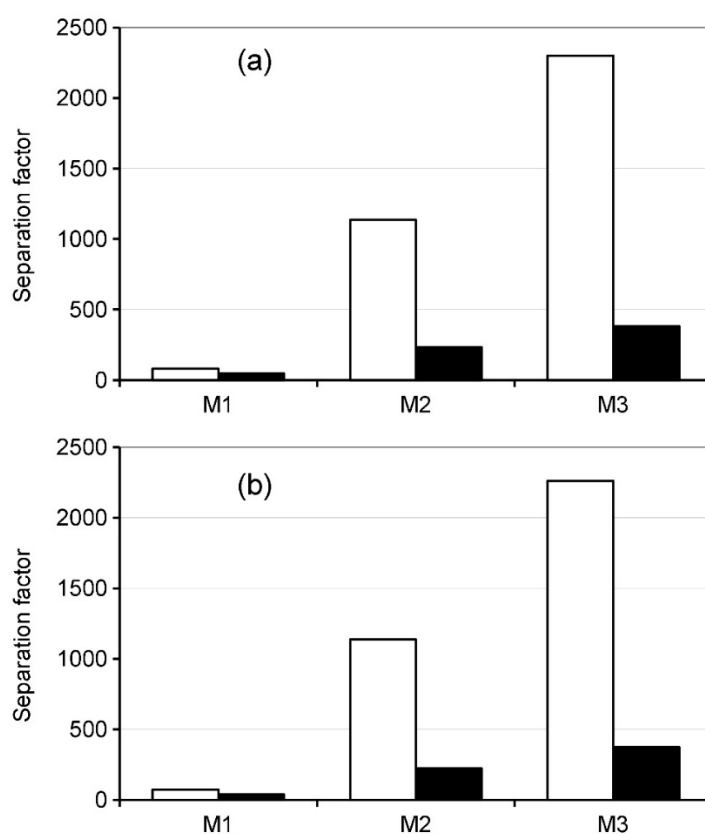


**Figure 11.** Separation factor of 10 wt % of water in water +isopropanol (white box) and water+ 1,4-dioxane (black box) feed mixtures vs. pristine PVA (M1), PVA/ $\text{Na}^+$ MMT-5(M2) and PVA/ $\text{Na}^+$ MMT-10 (M3) mixed matrix membranes at 30 °C for (a) thermally crosslinked membranes and (b) glutaraldehyde crosslinked membranes [120].

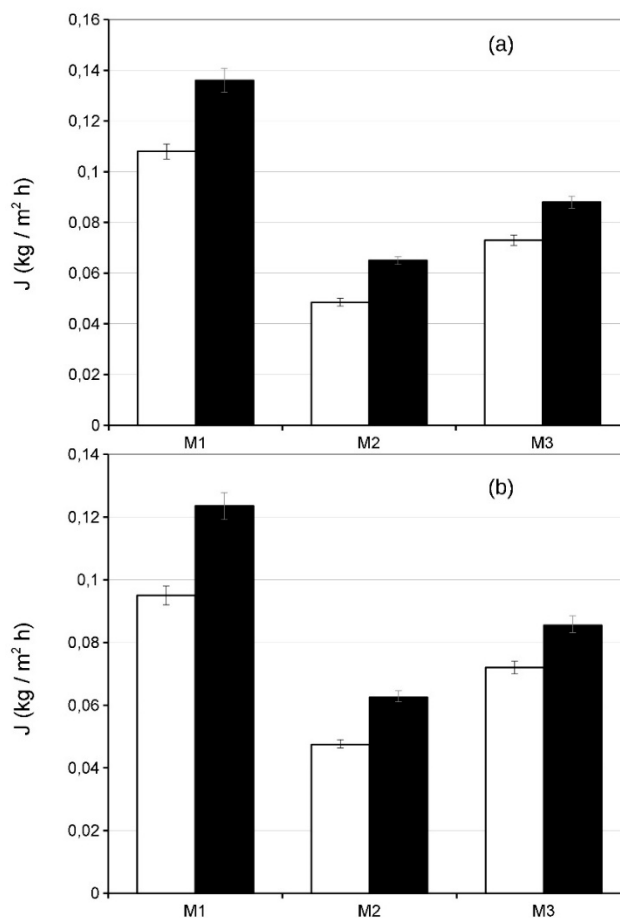


**Figure 12.** Water flux of 10 wt % of water in water+isopropanol (white box) and water + 1,4-dioxane (black box) feed mixtures vs. PVA (M1), PVA/Na<sup>+</sup>MMT-5(M2) and PVA/Na<sup>+</sup>MMT-10 (M3) mixed matrix membranes at 30 °C for (a) thermally crosslinked membranes and (b) glutaraldehyde crosslinked membranes [120].

Two MMMs were prepared by including 5 and 10 wt % of Na<sup>+</sup>MMT clay particles into PVA [120]. Membranes of this study have exhibited high separation factors and/or permeability to water from the chosen feed mixtures in addition to having sufficient mechanical strength properties. Membranes of this study showed high separation coefficients and/or permeability to water for various feed mixtures, and demonstrate adequate mechanical strength properties. Thus, after incorporating Na<sup>+</sup>MMT particles into PVA matrix, the membrane properties of PVA have greatly improved, including the pervaporation performance, more exactly, a separation factor. However, flux values of the membranes were somewhat lower in comparison with the unfilled PVA.

Generally, effects associated with the processes of the distribution of nanoscale inorganic particles in a polymer matrix are determined by the following factors: The amount and nature of the active groups in the polymer and in the filler, the presence in the polymer structure fragments—“potential ligands” for the filler used, as well as its size and structure [13,111,121]. As a rule, the polymeric components have not been specially designed to control interactions with the other ingredients. There is also a need for a more “wholistic” design of nanocomposites, whereby both polymeric and non-polymeric components should affect as reagents in solid-phase reactions [122,123].

Polyethersulfone (PES) with the incorporation of inorganic fillers of different shapes (Na-MMT clays—layers with two silica tetrahedral sheets sandwiching a central alumina octahedral sheet, and TiO<sub>2</sub> nanoparticles-spherical) were prepared and tested for CO<sub>2</sub>/CH<sub>4</sub> separation [124]. The study shows that the permeability of PES/MMT MMM to both gases, CO<sub>2</sub> and CH<sub>4</sub>, increased significantly

with increasing MMT content, that was accompanied by a dramatic decrease in selectivity. The main reason for this effect was called by authors as the appearance of voids and defects at the boundary of the polymer and inorganic phases. This phenomenon should be attributed to the big gas transport path created in the interface. Accordingly, the gas selectivity was far from the Robeson upper bounds (Figure 13). In particular, with a MMT content of 10% or more, the predominant mechanism of gas transport in these membranes is the Knudsen diffusion, so that  $\text{CO}_2$  and  $\text{CH}_4$  cannot actually be separated.

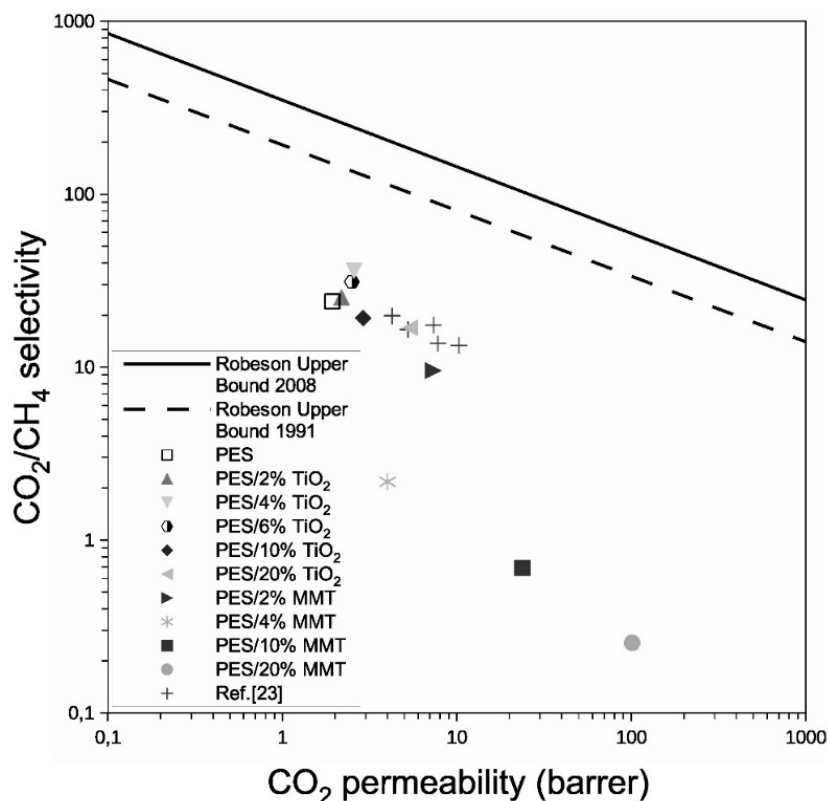


Figure 13. Performance of MMMs compared to the Robeson upper bounds [124].

The membranes with high MMT contents (more than 10 wt %) have some defects and, therefore, Knudsen diffusion with low separation ability became the predominant gas transport mechanism. In the case of PES/ $\text{TiO}_2$  MMMs, the  $\text{CO}_2/\text{CH}_4$  separation factor increased from 24.5 for pure PES membrane to 38.5 for 4 wt %  $\text{TiO}_2$  MMM and then decreased with a further increase in  $\text{TiO}_2$  content (17.3 for 20 wt %) (Figures 14 and 15). A reason is the same like in the case of MMT additive. SEM and TEM images revealed the inorganic filler agglomeration in MMMs. The size of the agglomerate becomes larger with a higher filler content, and at the interspace of the filler and the polymer, voids formed.

The conclusion was made that to improve the PES/MMT MMM performance, middle and micron size agglomerates as well as interface voids should be avoided. Some methods proposed in the literature may be useful for the production of MMMs with a more even distribution of MMT, less aggregation of particles and without defects at the polymer-inorganic interface, such as the ultrasonic treatment method for better distribution of the inorganic filler in the dispersion, the filler modification to improve its adhesion to the polymer, the use of organo-clays, melt processing in the membrane preparation, etc.

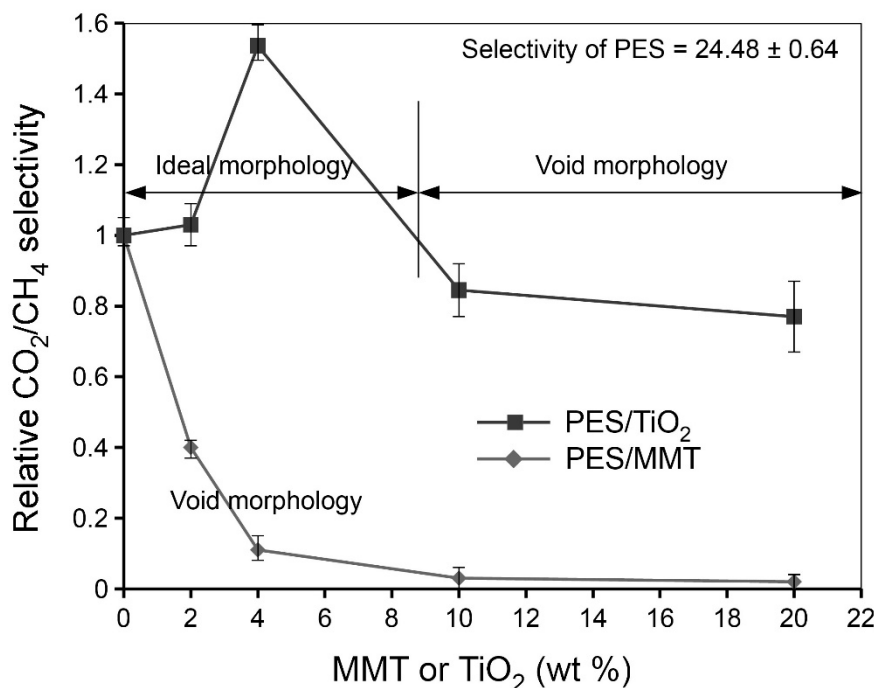


Figure 14. Relative CO<sub>2</sub>/CH<sub>4</sub> selectivity results for MMMs [124].

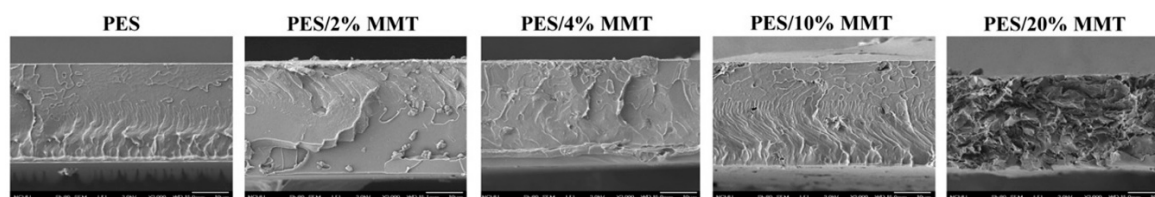


Figure 15. SEM photos for pure PES membrane and MMMs with different content of MMT.

The essential role of the particle/polymer boundary region was discussed in papers wherein colloidal silica was used as a nano-filler. It has been experimentally proven that the introduction of nano-sized colloidal silicon dioxide into the matrix of a highly permeable polymer significantly increases (up to an order of magnitude) the material's permeability in most cases [44,125–128]. In the case of nano-sized silica, penetrant solubility is known to have been unchanged for filler concentrations of up to 40–50 wt % [126]. Therefore, the observed increase in rate of penetration after incorporation of these nanoparticles in the polymer matrix should be associated with an increased diffusion rate of penetrants. An explanation was proposed [125] that the introduction of impermeable nanoparticles disrupts the packing of polymer chains near the surface of the filler. This leads to an increase in the free volume in the polymer-filler interphase region that was detected by positron annihilation life time spectroscopy [127] and <sup>129</sup>Xe NMR spectroscopy [128] on these highly permeable nanocomposites. Increasing the available free volume leads to faster diffusion through the layers of the interfacial polymer. Splicing interfacial layers with high penetration due to the clustering of nanoparticles can lead to the formation of long, highly permeable, preferred ways for penetrating diffusion. It was found that an increase in the surface area of the filler at its constant volume fraction in the composite, [125] results in a monotonic increase in the penetrant diffusion rate. This is further confirmation that the amount and properties of the polymer modified in the interphase region between the polymer and the filler are key factors determining the amount of gain in the diffusion permeability rate due to the addition of the filler to the polymeric membrane. The authors note that numerical methods, such as finite element method (FEM) and the recently developed material point method (MPM) can be

effective in the study of penetrant diffusion in heterogeneous media. In contrast to theoretical solutions based on assumptions about geometric arrangements and distributions over the sizes of different phases, numerical simulation can explicitly study the influence of shapes, sizes and effects of inclusion distribution on the properties of composites [125]. The main assumption of the authors [125] based on experimental data, was that the polymer membrane near the surface of nanoparticles enhances a diffusion of penetrants in comparison with the polymer material. In the model, this region of enhanced diffusion is treated as a “skin” on the nanoparticles which in themselves are considered to be impenetrable and are heterogeneously distributed in the polymer matrix.

Technology of forming and transport properties of nanocomposites based on latex and layered hydrosilicates depending on content of nano-fillers, surface treatment and nano-fillers distribution in polymer matrix, were investigated in Reference [129]. Transport barrier properties of nanocomposites relative to oxygen and nitrogen increased notably with the increasing of the nano-fillers content in comparison with unfilled polymer. When nanoparticles aggregate then the polymer-inorganic system became not the nano- but micro-composite with insignificant arising of barrier properties. Sometimes the anomalous increase in gas permeability was observed that was explained by the increasing of free volume owing to voids, as a result of nanoparticles aggregations.

It has been reported that, depending on the amount of filler used, the aspect ratio of the plates and the state of dispersion of the silicate particles and their orientation, a gas permeability reduction of 20 to 90%, is observed compared to the control of unfilled polymer and of 20 to 60% for nanocomposites based on MMT [113,130–134].

An obvious reduction in gas permeability was observed by the authors [4,130] in the study of polymer-filled composite materials containing nanoparticles of MMTs or synthetic hydrosilicate NTs with chrysotile structure (SNT, Figure 16a,b) [130,135]. SNTs ( $Mg_3Si_2O_5(OH)_4$ ) synthesized under hydrothermal conditions crystallographically and are morphologically similar to the nano-fibrils of a natural asbestos but are considerably shorter [130,136]. SNTs containing polyimide nanocomposites were prepared by solution mixing-casting method.

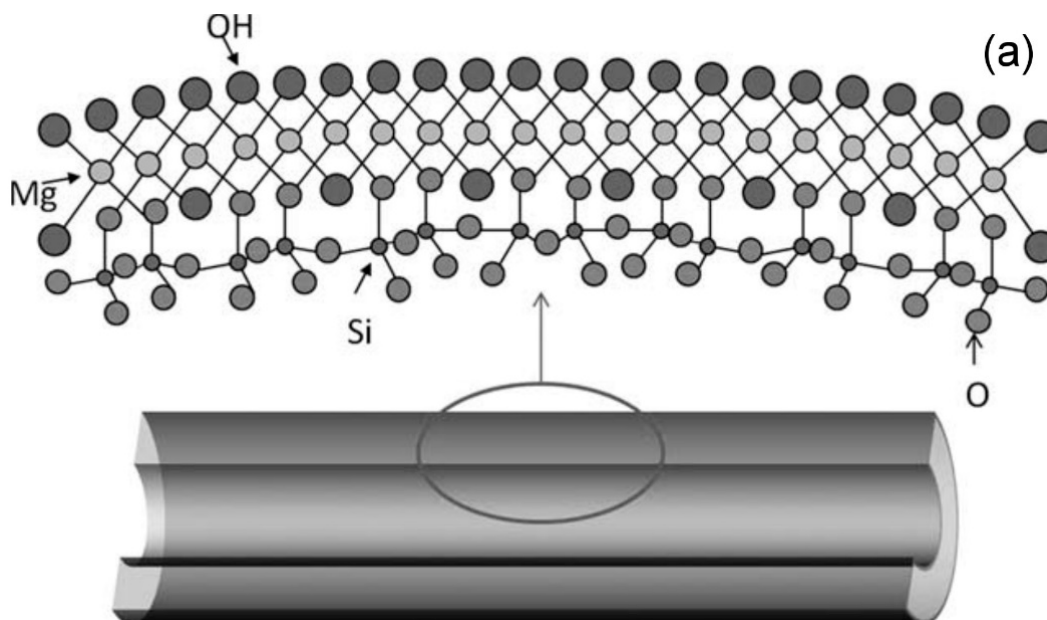
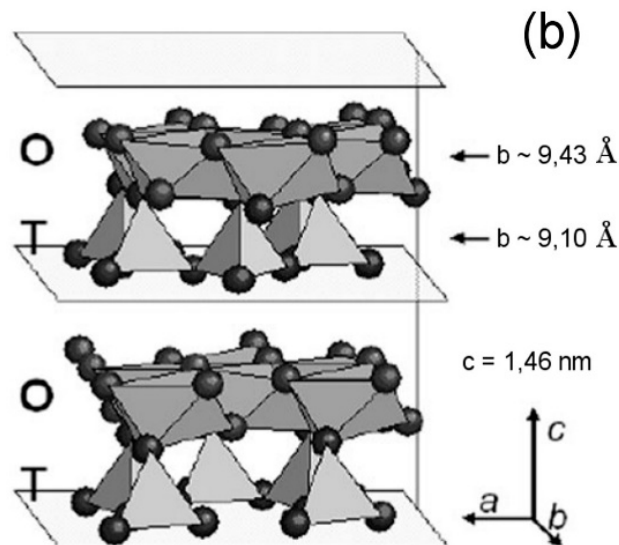


Figure 16. Cont.



**Figure 16.** (a) Scheme 1 of the chrysotile hollow tube structure:  $85 \times 53$  mm ( $300 \times 300$  DPI) [130]; (b) lattice of chrysotile (Scheme 2 [135]).

The introduction of the inorganic phase into the polymer enhances the gas barrier of the polymer. This fact, according to the authors, is associated with a more tortuous diffusion pathway. Oxygen permeability decreased by 24% for PI PAA-PM/SNT containing 4.1 vol % SNT and by 40% for PI PAA-PM/SNT containing 19.6 vol % SNT. Contrary to expectations, the decrease in water vapor permeability due to the addition of SNT to the polymer was less than the decrease in oxygen permeability. Permeability for water vapor decreased by 1.5% for PIPAA-PM/SNT with 4.7 vol % SNT and 29% for PIPAA-PM/SNT with 19.6 vol % SNT.

The SEM micrograph of the surface of the PIPAA-PM/SNT nanocomposite films obtained (Figure 17) shows a homogeneous dispersion of SNT in the polymer matrix and existence of nanoparticles on the upper membrane surface.

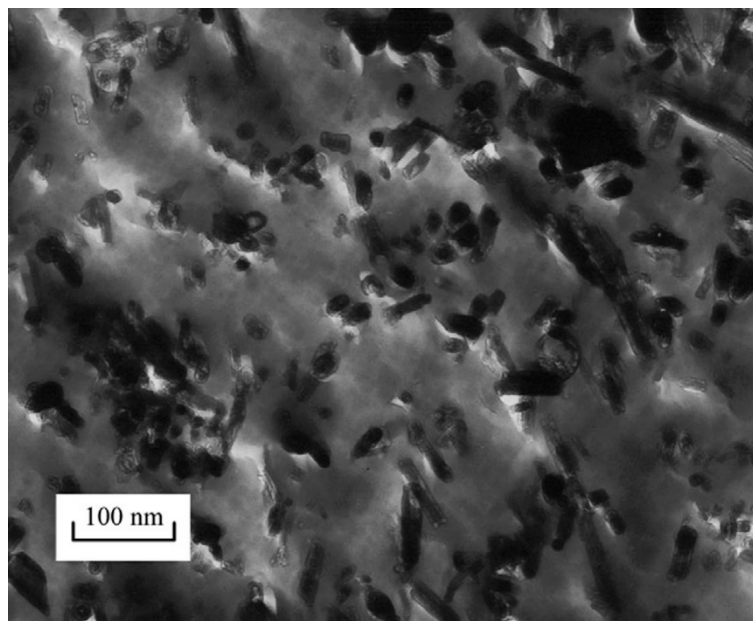


**Figure 17.** SEM photomicrograph of the surface of PIPAA-PM/SNT nanocomposite film (volume fraction of SNT is 19.6%) [4].

Figure 18 illustrates the relative permeability of oxygen as a function of the volume % SNT in PIPAA-PM/SNT nanocomposite films. The curves represent the theoretical barrier behavior of composites filled with particles of different geometries: Randomly distributed spheres (curve 1), randomly distributed disks aligned perpendicular to the direction of penetration with aspect ratio  $r/h = 10$  (curve 2), uniformly distributed rods with a random and homogeneous distribution in the plane, perpendicular to the direction of permeability with  $L/d = 1$  (curve 3), 5 (curve 4) and 20 (curve 5). The relative gas permeability of composites filled with impermeable spheres was predicted using the Maxwell equation,  $P_{NC}/P_M = (1 - \phi)/(1 + \phi/2)$ , where  $P_{NC}$  is the permeability of the composite medium and  $P_M$  is the matrix permeability,  $\phi$  is volume fraction of impermeable phase.

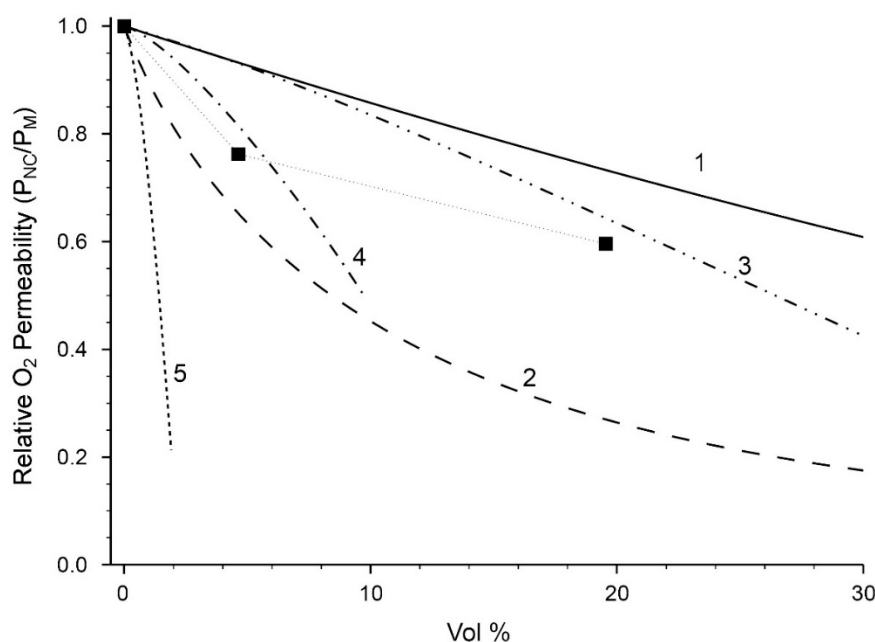


**Figure 18.** Relative oxygen permeability as a function of vol % of SNT in PIPAA-PM/SNT nanocomposite films. The curves represent theoretical predictions of composites filled with fillers exhibiting different geometries: spherical (1), disks with  $r/h = 10$  (2), and rods with  $L/d = 1$  (3), 5 (4) and 20 (5). Note that subscripts NC and M in the y-axis legend represent PIPAA-PM/SNT and PIPAA-PM, respectively, as described in the text [4].

Relative permeability of composites filled with aligned disks was predicted using the Nielsen's equation,  $P_{NC}/P_M = (1 - \phi)/(1 + (f \times r/h))$ , where  $r$  is the disk radius and  $h$  is the disk thickness. Relative permeability of rods was predicted using an expression derived by Fredrickson and Shaqfeh. Figure 18 shows that theoretically the oxygen permeability for PIPAA-PM/SNT tends to decrease between the value for a composite filled with random spheres and the value for a composite filled with randomly distributed disks characterized by a  $r/h = 10$  aspect ratio and aligned perpendicularly to the direction of penetration. The authors emphasize that the ratio  $r/h \sim 5-10$  is a characteristic value of typical mineral additives such as talc, calcite and kaolin. It was found that the values of the oxygen barrier for all the PIPAA-PM/SNT systems studied were significantly lower than the predicted theoretical values, assuming that the rods were randomly dispersed, but aligned with the aspect ratio 20 (curve 5). The aspect ratio  $L/d = 20$  represents the characteristic dimensions of SNT nanoparticles, which were used in the work under discussion,  $L \sim 400$  nm and  $d \sim 20$  nm (Figure 18).

The question arises as to why the experimentally measured gas barrier PIPAA-PM/SNT turned out to be lower than the theoretical prediction depicted by curve 5 in Figure 18? According to the authors, one possible reason for this discrepancy is that the SNTs are not aligned exactly in a plane perpendicular to the direction of penetration, which is one of the central assumptions of the model.

Another reason for the discrepancy mentioned above is related to the probability of change in the aspect ratio of the nanoparticles actually introduced into the polymer due to the selected conditions for the formation of the composite. For example, brittle failure of CNT as a result of ultrasonic treatment is possible.

The barrier of oxygen and water vapor of nanocomposite films was studied in Reference [130], depending on the amount of chrysotile NTs, the degree of their dispersion, and the orientation in the matrix (Table 1). The dispersion characteristics and orientation of NTs were examined by transmission electron microscopy (TEM, Figures 19 and 20).

**Table 1.** Oxygen and water vapor barrier characteristics of polyimide/SNT nanocomposites [130].

wt %	vol %	P (Oxygen)		P (Water)		D (Oxygen)		S (Oxygen)	
		[cc(STP) cm m <sup>-2</sup> day <sup>-1</sup> atm <sup>-1</sup> ]	[cc(STP) cm m <sup>-2</sup> day <sup>-1</sup> atm <sup>-1</sup> ]	[cc(STP) cm m <sup>-2</sup> day <sup>-1</sup> atm <sup>-1</sup> ]	[cc(STP) cm m <sup>-2</sup> day <sup>-1</sup> atm <sup>-1</sup> ]	[10 <sup>-9</sup> cm <sup>2</sup> s <sup>-1</sup> ]	[10 <sup>-9</sup> cm <sup>2</sup> s <sup>-1</sup> ]	[cc(STP) cc <sup>-1</sup> atm <sup>-1</sup> ]	[cc(STP) cc <sup>-1</sup> atm <sup>-1</sup> ]
0	0	1.42 ± 0.06		2328 ± 116		2.3 ± 0.3		0.73 ± 0.07	
2.9	1.6	1.16 ± 0.05		-		1.8 ± 0.2		0.73 ± 0.07	
3.9	2.2	0.942 ± 0.04		1957 ± 80		1.6 ± 0.2		0.69 ± 0.07	
4.8	2.7	0.905 ± 0.04		1443 ± 72		1.5 ± 0.2		0.72 ± 0.07	
6.5	3.7	0.542 ± 0.02		1365 ± 68		1.2 ± 0.1		0.54 ± 0.05	
7.0	4.0	0.539 ± 0.02		1209 ± 61		1.1 ± 0.1		0.55 ± 0.06	
7.8	4.5	0.505 ± 0.02		965 ± 48		1.1 ± 0.1		0.56 ± 0.06	
9.1	5.3	0.851 ± 0.03		1463 ± 73		1.6 ± 0.2		0.60 ± 0.06	
13.0	7.7	0.849 ± 0.03		1363 ± 68		1.8 ± 0.2		0.55 ± 0.06	
16.7	10.0	0.788 ± 0.08		1239 ± 62		2.0 ± 0.2		0.45 ± 0.05	

The SNTs were well dispersed and oriented in the film plane in nanocomposites with a tube concentration of up to 4.5% (*v/v*), which led to a gradual increase in the gas barrier. The lowest gas permeability was 60% less than that of the original polyimide film. However, the microaggregation of nanoparticles in dispersions and their orientation were initiated at high SNT loads, and the oxygen barrier was reduced. The dependence of the permeability on the volume concentration of NT has an extreme character and is presented in Figure 21.

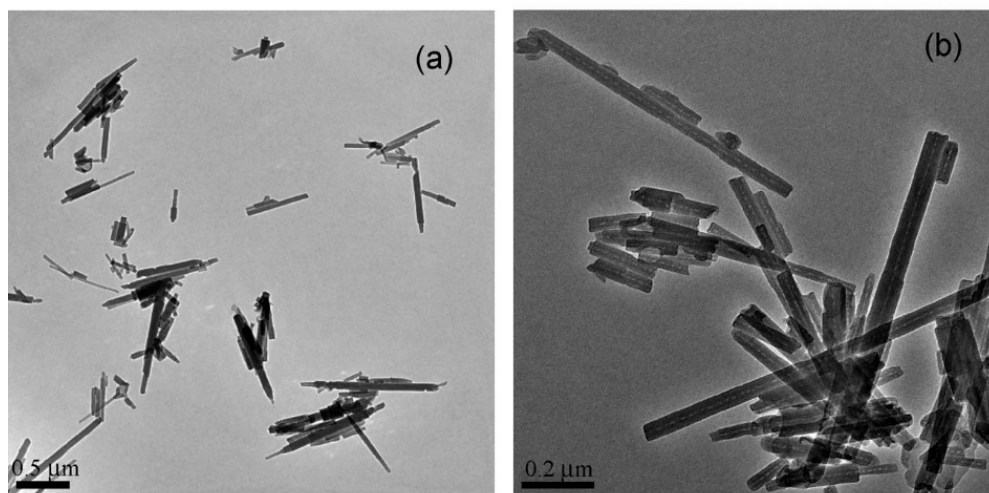


**Figure 19.** TEM of the NTs obtained at various magnifications: (a) Low and (b) High. 85 × 173 mm (300 × 300 DPI) [130].

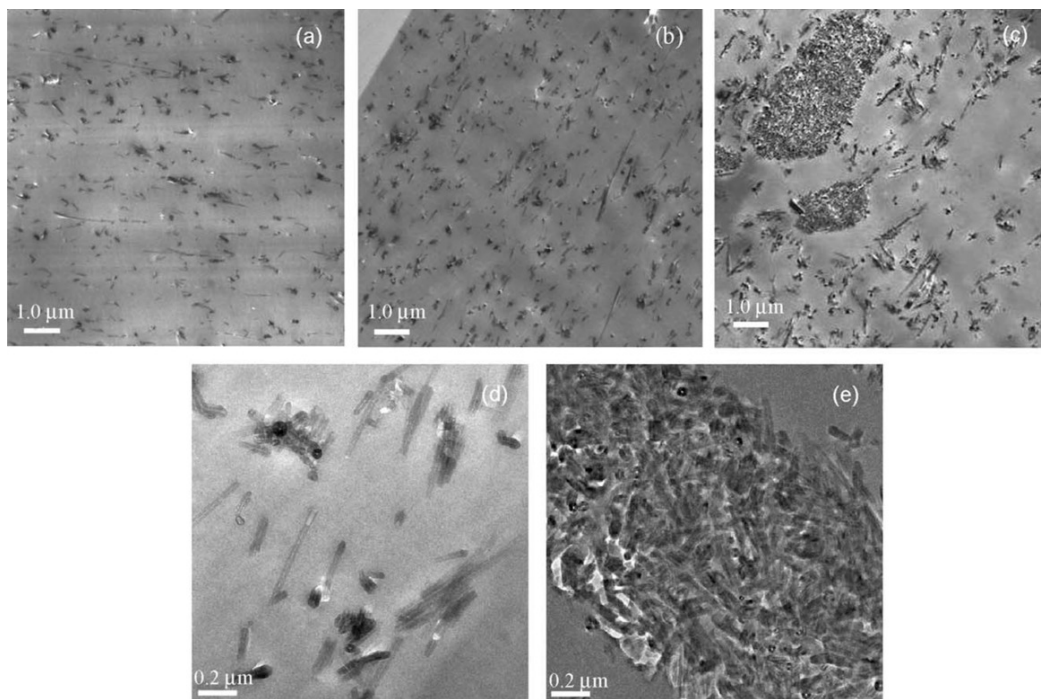


**Figure 20.** TEM micrographs of microtomed nanocomposites containing various NT loadings: (a) 2.2% (vol/vol); (b) 4.5% (vol/vol); (c) 7.7% (vol/vol)—low magnification; (d) 4.5% (vol/vol) and (e) 7.7% (vol/vol)—high magnification [130].

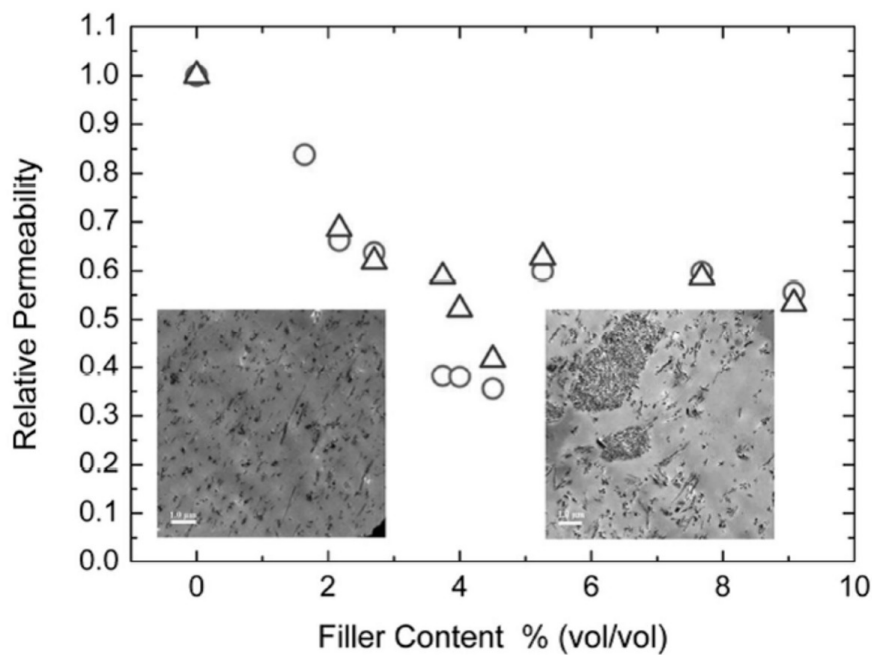


**Figure 21.** Chrysotile nanotubes (ChNTS = SNT) containing polyimide nanocomposites were prepared by solution mixing-casting method [130].

At smaller SNT compositions, the NTs were nano-dispersed and in-plane orientated, thus leading to higher gas barrier. The lowest oxygen permeability found for the nanocomposites was at 4.5% (vol/vol) of NTs and it was 64% smaller than for the pristine polyimide. However, with the onset of NT micro aggregation the NT dispersion and orientation were markedly compromised and the oxygen

barrier was noticeably reduced. The reduction of the oxygen permeability at a smaller SNT content was essentially due to diffusivity while the contribution of oxygen solubility was minor. At larger SNT content, however, the relative contributions of oxygen diffusivity and solubility were comparable. The solubility trend at larger NT compositions indicated the possibility of excluded, screened within the nano—aggregates (bundles) and micro aggregates, and thus insoluble polymeric regions.

When two dependences of the relative permeability of oxygen and water (normalized to the permeability of unfilled polyimide) were presented on one graph, relative to the volumetric SNT composition, it was assumed that the observed penetration behavior is not specific for the gas (vapor) and reflects a structural change only within the nanocomposites. In accordance with Nielsen's formula, nanocomposites based on SNT and nanocomposites with nanodispersed and randomly oriented layers of silicate MMT showed comparable gas barriers at small concentrations of nanoparticles [130].

(VIII) It is known that the typical results of introduction of inorganic particles in the polymer which leads to a decrease in mass transfer zone [112,130]. As was discussed above, structure of NTs, their shape, length, ratio of inner and outer diameters, and surface chemistry can influence the morphological features of the composites. Of particular interest in this context was the development of new composite materials based on aromatic polyamide-imides (PAIs), with inorganic particles of a chrysotile structure as fillers.

MMMs were prepared by a solution mixing-casting method using ultrasonic agitation of poly(diphenyloxydeamide-*N*-phenyl phthalimide) (PAI-1) dispersions with SNT [112]. The duration of the mixing process (up to 20 h) was determined by the required degree of homogeneity of the resulting composites. The content of the inorganic components was varied from 2 to 10 wt % [112].

It should be pointed out that there is a significant difference between the composite material PAI-1-SNT and typical composites “polymer-inorganic fillers of SNT type” in terms of selectively increasing permeability of PAI-1 after incorporating NT [112]. The following inorganic fillers were used in the composites: natural montmorillonite intercalated with quaternary aliphatic amine; commercial product Cloisite 15A (Southern Clay Products, Inc., Gonzales, TX 78629 USA); and SNT of  $Mg_3Si_2O_5(OH)_4$  with a chrysotile structure. These SNTs were produced by hydrothermal synthesis [137,138] and have a cylindrical morphology and various dimensions: (a) outer diameter  $d_o = 10\text{--}15$  nm, inner diameter  $d_i = 2\text{--}3$  nm, and length  $L = 100\text{--}250$  nm (SNT-I); (b)  $d_o = 20\text{--}25$  nm,  $d_i = 4$  nm, and  $L = 500\text{--}1000$  nm (SNT-II); and (c)  $d_o = 50\text{--}110$  nm,  $d_i = 5\text{--}6$  nm, and  $L = 300\text{--}700$  nm (SNT-III) (Figure 22a–c).

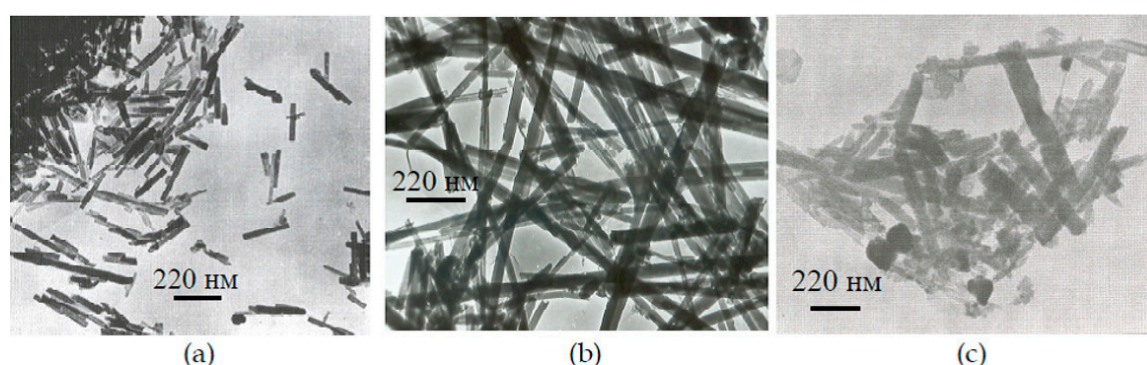


**Figure 22.** Micrographs of  $Mg_3Si_2O_5(OH)_4$  SNTs with a cylindrical morphology and various dimensions: (a) SNT-I; (b) SNT-II; and (c) SNT-III [112].

The photomicrographs of the film's surfaces showed that the surface relief of PAI-1-SNT is similar to the corresponding reliefs of homogeneous film of PAI-1 (Figure 23). Both composite and PAI-1 homogeneous films are characterized by a smooth upper surface and finely granular lower one, on which are viewed clearly expressed bands, not related to the presence of an inorganic component in the composite.

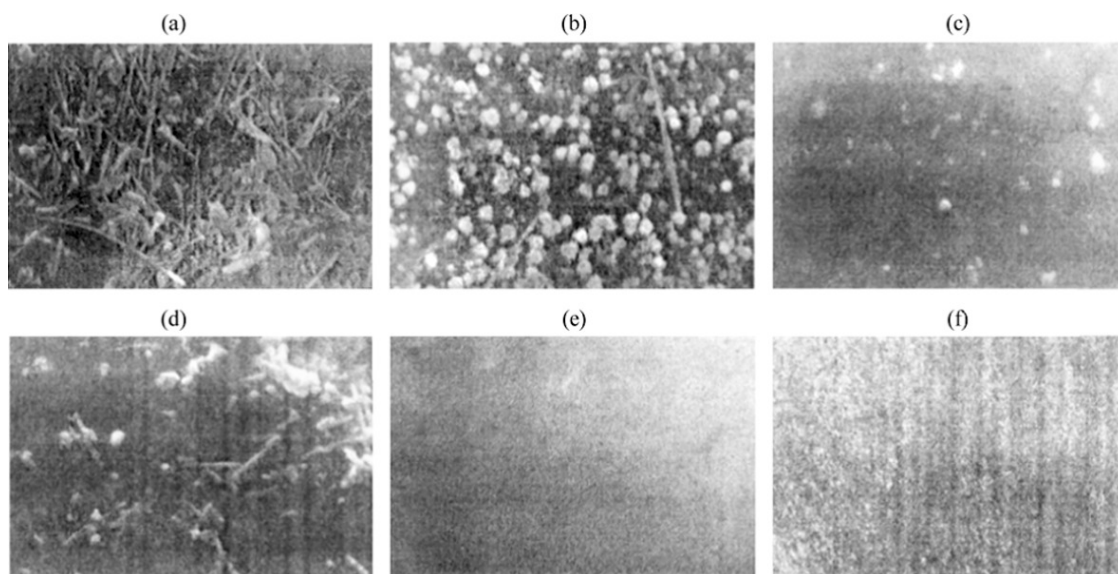


**Figure 23.** SEM micrographs of (a,b,e) upper and (c,d,f) lower surfaces of (a–d) PAI-NTII(10) and (e,f) PAI-NTII(20) of thickness 20  $\mu\text{m}$  [112].

A study of the transport properties of the corresponding films (homogeneous membranes) in pervaporation demonstrated the following. Introduction into the polymeric matrix NTs of the SNT-I–III types without their additional treatment (chemical or orienting) leads to an increase in the flux of water across the corresponding film membrane (Table 2 sample nos. 2–4 [112]), which is the most pronounced for SNT-II in the case of a good compatibility of components of the composite material (Table 2, sample N 3).

**Table 2.** Permeate flux for water,  $P_w$ , and flux normalized to thickness for non-porous composite films in comparison with a nonporous PAI film (sample No. 1) in pervaporation at 40  $^{\circ}\text{C}$  [112].

Sample No.	Sample	c, wt %	$l^*$ , $\mu\text{m}$	$P_w$ , $\text{kg m}^{-2} \text{h}^{-1}$	$P_w l^*$ , $\text{kg m}^{-2} \text{h}^{-1} \mu\text{m}$
1	PAI	0	15	0.043	0.645
2	PAI-SNT I	2	15	0.044	0.660
3	PAI-SNT II	10	15	0.084	1.260
4	PAI-SNT III	2	15	0.056	0.672

\*  $l$  is the sample thickness, and  $P_w l$  is sample flux normalized to thickness.

Table 3 [112] compares the results of tests of PAI-1 and PAI-1-SNT-II(20) (20 min of ultrasonic agitation, 2 wt %) films, and of a composite PAI-1-MMT-15A (2 wt %) film obtained under the conditions in which PAI-1-SNT-II(20) was formed, in dehydration of an aqueous solution of ethanol (48 wt % ethanol) in the course of pervaporation at 40  $^{\circ}\text{C}$ . As the content of NTs in the composite increases from 2 to 10 wt % (Table 3, sample N 5 and Table 2, sample N 3, respectively), the permeability of the material to polar liquids, such as water and ethanol, grows. A possible explanation of this effect is that the permeability is affected by the appearance of microscopic inhomogeneities or defects (on the nanosize level or coarser) in the nonporous matrix of the composite film upon introduction of the inorganic component. However, this assumption is easily refuted by analysis of the data in Table 3, because introduction of 2 wt % SNT-II into a PAI-1 film yields a composite for which the separation factor of the water/ethanol mixture not only does not decrease, but even somewhat increases as compared with that for the homogeneous PAI-1 film.

**Table 3.** Permeability to water of nonporous films of PAI-SNT I-III composites, in comparison with the nonporous PAI film, in pervaporation at 40 °C [112].

Sample No.	Sample	c, wt %	l, $\mu\text{m}$	P, $\text{kg m}^{-2} \text{h}^{-1}$	$F_w$
1	PAI	0	15	3.20	5.5
5	PAI-NT II	2	15	3.75	7.9
6	PAI-MMT-15A	2	15	2.35	5.8

\*  $l$  is the sample thickness, and  $P/l$ , sample permeability normalized to thickness.

In this property (an increase in permeability to liquids upon introduction of inorganic nanotubular additives), the PAI-1-SNT-II (20) composite material obtained strongly differs from typical composites constituted by a polymer and an inorganic filler. As a rule, introduction of inorganic particles into a polymeric matrix results in an inorganic phase impermeable to gases and liquid is formed in the matrix and the mass-transfer zone becomes narrower. As a result, the permeability on nonporous films falls. For this reason, introduction into the PAI-1 matrix of 2 wt % MMT-15A particles under the same conditions yields a composite material with lowered permeability, as shown in Table 3. Because inorganic MMT-15A particles and SNT are close in chemical composition, no other components are present in the systems under consideration, and the formation conditions were similar, it can be assumed that the nano-size structural features of the films exert a decisive influence on their transport properties.

The properties of the filled polymers resulting from the processes of distribution of nano-sized inorganic particles in them appear to be determined not only by the new structural characteristics of the composites, but also by factors such as the number and nature of the reactive groups of the components, and also the presence of fragments in the polymer structure that can serve as “potential ligands” for the selected filler. Therefore, a comparative study was of interest of the structure and transport properties of nanocomposites formed by the introduction of inorganic NTs into the polymers of different chemical structure. The non-porous composite films based on the aromatic PAIs differing by the structure of diamine component containing equal amounts of SNT were obtained and investigated in dependence to the structure and transport properties [121].

The main reason for the choice of these nanoparticles was the chemical composition of their surface, namely, the presence of the reactive polar hydroxyl groups. Moderately hydrophilic PAIs, characterized by the ability to interact with the functional groups of magnesium-SNTs, as well as to interact with the solvents used as penetrating substances, were studied in the pervaporation process. It became possible to study the influence of functionalization of the polymer matrix on the morphological and transport properties of formed nanocomposites.

In the paper [121], the transport properties of PAI-1 and PAI-1-SNT were examined at the pervaporation in relation to a wide range of penetrating substances (water, methanol, cyclohexane, and methyl-*tert*-butyl ether). It is unclear up today how is formed and where is located the “priority transport channel” for the more polar components of the penetrating mixture. An assumption seems correct about the special role of the hydroxyl-groups located on the outer surface of the used SNT, that it is able to interact with both amide and imide groups of the PAI-1, and with the polar groups of the transported molecules (water, alcohols). If this assumption was correct, then the introduction in the polymer chain of the functional groups capable to form hydrogen bonds with hydroxyl-groups or water dipoles should affect the transport properties of the composites.

To test this hypothesis, the composite PAI-2-SNT-II that differs from PAI-1-SNT-II by the structure of the polymer diamine component and contains carboxy-groups of diaminobenzoic acid (PAI-2) was obtained. Figure 24 shows microphotographs of (a) upper and (b) lower surfaces of the film PAI-2-SNT-II. It was shown that, as in the case of PAI-1-SNT-II, the lower surface of the film has a distinct grain structure, unlike the smoother upper surface. On both surfaces at the zoom 18,000 NTs were not found freely “lying”, nor their fragments. All NTs were in the inner layers of the composite film.

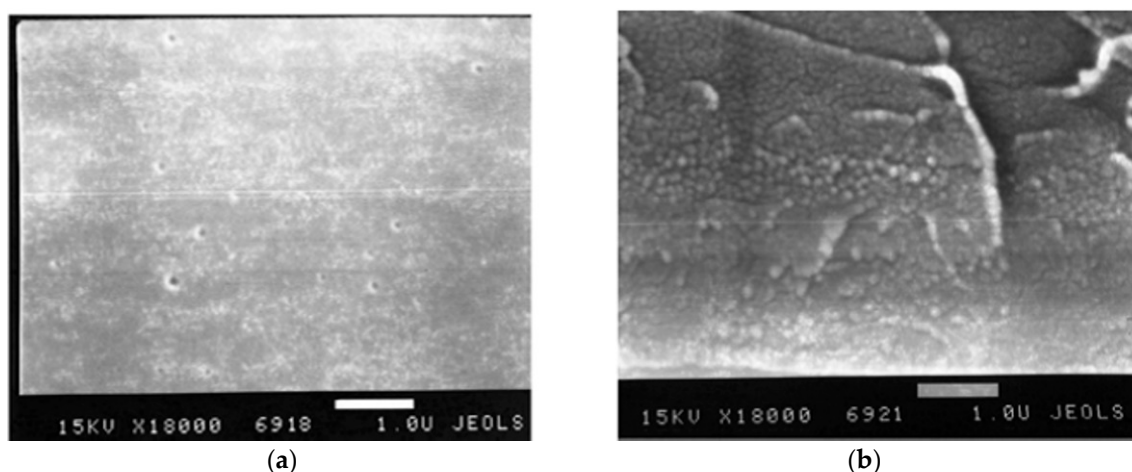


**Figure 24.** The composite PAI-2-SNT-II: SEM of (a) Upper; (b) Bottom surfaces [121].

PAI-2 being more of a hydrophilic polymer is two times more permeable by water than PAI-1, like in the case of PAI-1-SNT, compared to PAI-1. The introduction of NTs in the PAI-2 enhances the ability of the film to pass water more than two-fold, which makes the material five-fold more permeable for water than PAI-1-SNT. It should be noted that the permeability of PAI-2-SNT by a low polar penetrant cyclohexane remain as low as the permeability of PAI-2, in contrast to PAI-1, for which the introduction of NTs reduces the permeability of cyclohexane significantly (Figure 24).

Most important is the fact that the composites PAI-1-SNT and PAI-2-SNT are obtained under similar conditions and containing NTs in equal amounts, they are similar by the trend of permeability of polar and weakly polar liquids, but differ by their degree.

The effect obtained requires attention and explanation. It is obviously associated with the appearance of a channel with facilitated transfer of the dipoles of water molecules or polar alcohols in the moderately swelling matrix of the composite film. The nature of interaction of the polymer matrix with the nanoparticles, which determines distribution of the latter in the nanocomposite film, affects the transport channel formation. In other words, the difference in the structure of the films on the nano-scale level leads to a difference in their transport properties. Figure 25 shows ultrafine cross-sections of PAI-1-SNT and PAI-2-SNT films, allowing us to judge about the nature of NTs and their agglomerates distribution in the inner layers of membranes. The image analysis shows that unlike the PAI-1-SNT film, which is characterized by aggregates of 10 NTs randomly placed throughout the thickness of the sample, in the PAI-2-SNT the aggregates are observed of 2–3 NTs that are uniformly distributed in the inner layers of the film. Aggregates containing the same numbers of NTs were also observed by AFM methods [139]. These morphological features correlate well with the data on pervaporation presented in this paper.

Selective increase in permeability, instead of barrier properties, for cases of introduction of SNT into the polymer, but simultaneous decrease in permeability of PAI-1-SNT—these data indicate the possible realization of the sieving effect due to the structural features of nano-fillers, as it was well shown above on the example of zeolite-polymer systems. However, an increase in water permeability and a decrease in cyclohexane permeability may be due to sieving (in terms of the size of the molecules) or to physical interactions between the nanoparticles and the penetrant, and thus influencing the transport of liquid penetrants by the sorption-diffusion mechanism (Figure 26). In the latter case, the presence of OH groups in NT should influence the transport of water. It should be noted that these groups are absent in the inner channel of the NT and are in the upper surface and interlayer space of the tube-roll (Figure 16 [130]). In the MMT structure there are also OH groups available for interactions, but in a smaller amount. However, water permeability only decreases when passing from non-porous

PAI-1 films to PAI-1-MMT composite films, as is typical for many polymer-MMT systems and was discussed in detail above.

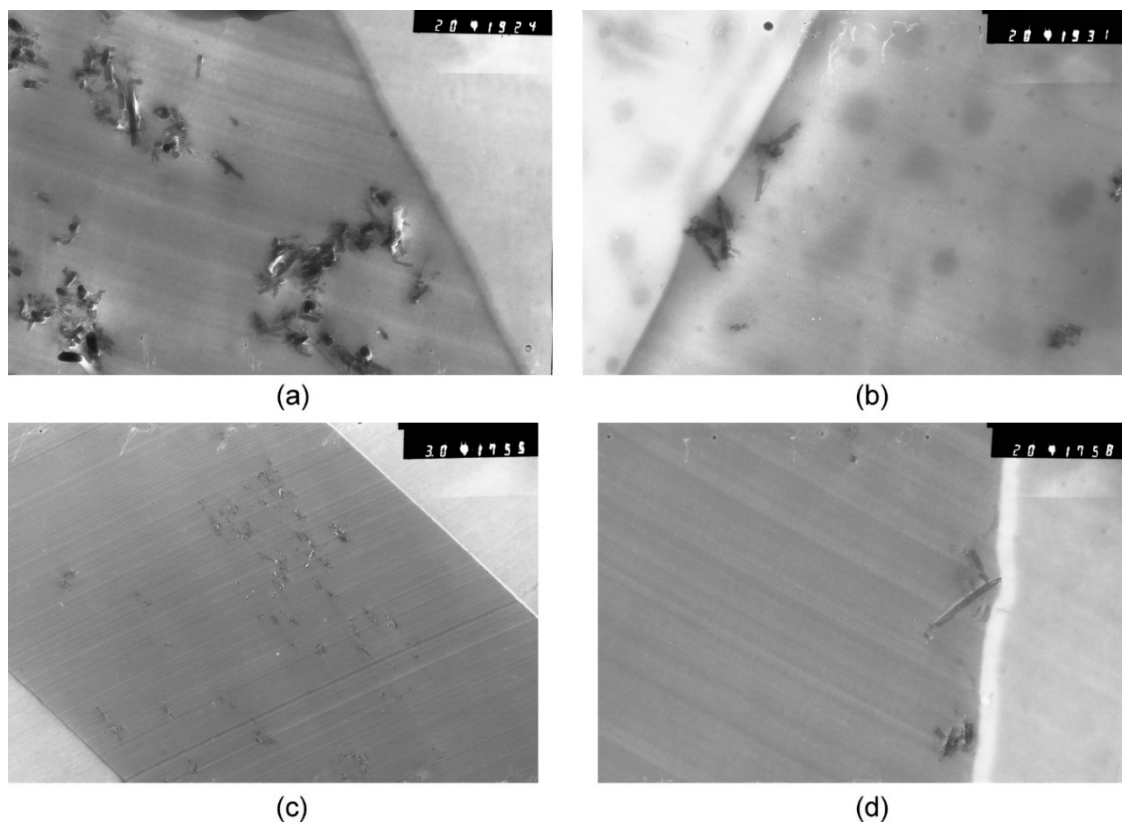


**Figure 25.** Photomicrographs of ultra—thin cross—cuts for (a,b) PAI-1-SNT-II and (c,d) PAI-2-SNT-II. Magnifications: (a,b,d) 2000; (c) 3000 [121].

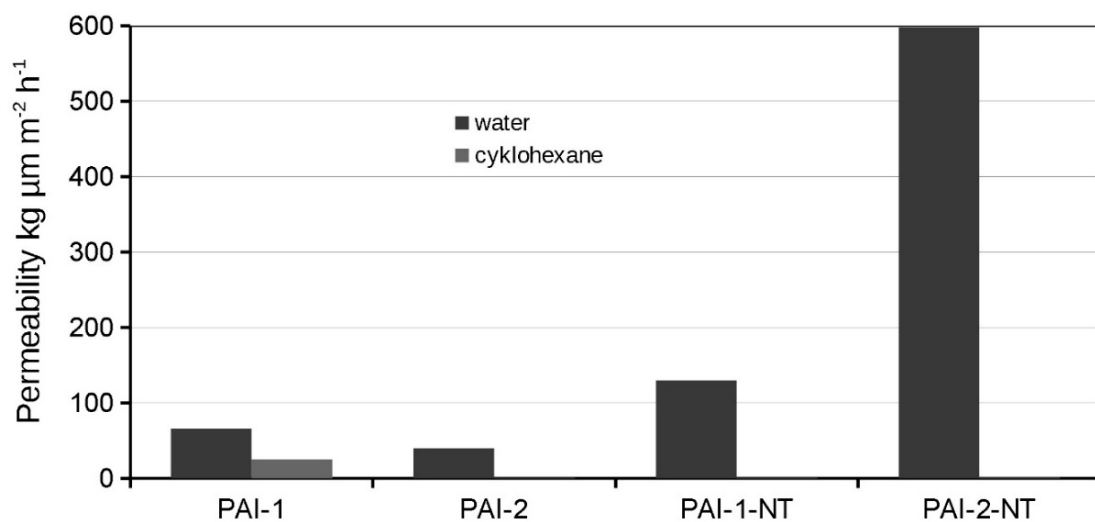


**Figure 26.** Permeability by water and cyclohexane (at 40 °C) of non-porous membranes PAI-1, PAI-1-NT, PAI-2, and PAI-2-NT [121].

The introduction of SNT into polyamide-imide films (PAI-1 or PAI-2) changes the properties of these polymers, that was showed in Reference [29] and this effect was studied in References [140,141].

It is important that the properties of PAI-1 change completely differently from the properties of PAI-2 when introducing the same nano-filler-SNT in the same quantities under the same conditions.

The data presented in the publications [29,112] show and clearly illustrate the differences in properties given by the nano-filling. At the same time, there is no single-valued correlation between these changes and transport properties. Thermal stability and Tg of composites based on PAI-1 with 2 wt % SNT were investigated by TGA and DSC [142]. It was shown that composites had a higher glass transition temperature as compared with that of PAI-1 (275 and 291 °C).

Equally bright changes in the state of the polymer matrix were observed earlier in polymer-nano-filler systems and are well described [1,143]. With inorganic particle and nanoparticle inclusions, nucleation of crystallization can occur. Nanoparticles can replace the absence of primary nuclei, thus promoting crystallization. At higher nanoparticle content, the increased viscosity (decreased chain diffusion rate) can lead to decreased crystallization kinetics. In this case, the crystallization process is influenced by several competing factors. For crystallization nanocomposites based on layered clay silicate it was noted that the nucleation occurs in many systems to reduce the overall crystallization rate, especially at higher amounts of nanoclay content [1,143]. The influence of different types of carbon nanoparticles on the recrystallization process of polyimide R-BAPB was studied [144]. It was proved that the nucleating effect of carbon nanoparticles depends strongly on their inherent crystallinity. Graphitic nanoparticles already at a low concentration of ~1 vol % induce the nucleation of polyimide R-BAPB.

The polymer structure and dynamics are known to have a great influence on small penetrant diffusion. The important question of the “nano-effect” of nanoparticles or fibers after their inclusion in a polymer-based composite film is addressed relative to crystallization and glass transition behavior [1]. It was shown, in many the cases nanocomposites studied could be approximated using a model of a continuous medium, thus “nano-effect” was not observed. This should not be surprising, since the size of the gas molecules penetrating were still significantly lower than the modification of nanoscale. Nanoscale is considered where the dimensions of the modifying particles, plates or fibers are in the range of 1–100 nm. The differences would be expected in those cases where glass transition temperature (Tg) of the matrix polymer changed. In other words, “nano-effect” noted in the literature has been the change in the Tg of the polymer matrix with the addition of nano-sized particles. Both increasing and decreasing in the Tg have been reported dependent upon the interaction between the matrix and the particle [1].

The difference in the state of the PAI-1 and PAI-2 matrices after introducing the same (including in size and morphology) SNT into the same conditions is also accompanied by a difference in the sizes of the formed agglomerates (an average of 10 nanoparticles in the agglomerate from SNT is formed in the case of PAI-1, and on average 2 NTs in the agglomerate—in the case of PAI-2) [112,142]. Of course, the interaction between the SNT and the polymer of the matrix, perhaps connected with the formation of hydrogen bonds, for example, –OH . . . HOOC– in the case of PAI-2, plays a role. This effect is well manifested in the difference in adhesion between SNT and PAI and was illustrated in Reference [142].

It is important that a comparative study of nanocomposite properties was carried out for samples with low concentration of nanoparticles, when nano-fillers were not observed on the upper surface. Consequently, one could not speak of significant changes in the adsorption separation factor. At the same time, changes were detected in the structural and morphological characteristics of the polymer component of the composite film.

Thus, adhesion to SNTs in the transition from PAI-1 to PAI-2 increases. When SNTs appear on the surface of films, the adhesion between the matrix and the filler is violated, which is confirmed by the AFM data (Figure 27). In this case, both transport and strength properties of composites are reduced [142]. At 2% SNT content, they are regularly distributed in the matrix in the form of small groups. In the near-surface layers of the composite they are coated with a polymer as shown in Figure 25c,d. Surfaces of the PAI-2 and the PAI-2-SNT composite films are significantly different.

So instead of craters from the solvent on topography of the surface, the new formations in the form of hills are observed [29].

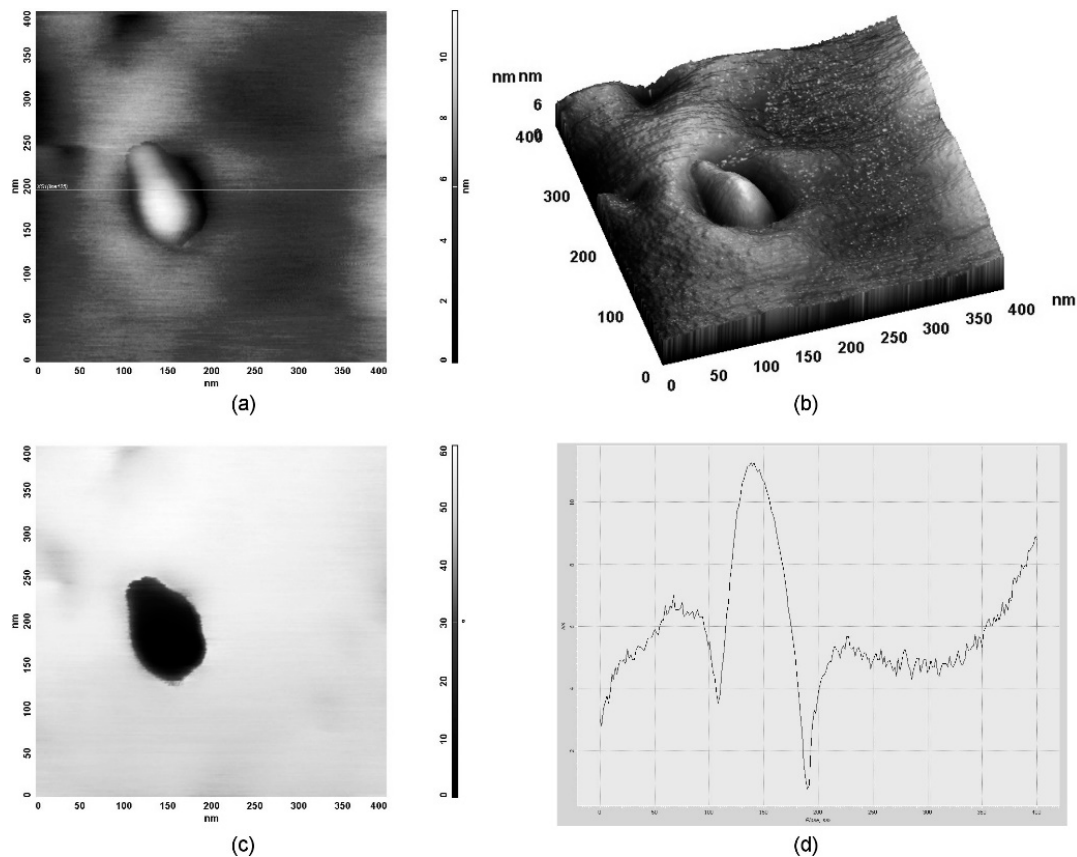


**Figure 27.** AFM-images of magnesium hydrosilicate NT on the surface of polymer matrix at 5 wt % of nano-filler content: topography (a); 3D image (b); phase contrast (c) and profile (d) [142].

The presence of micro-voids at the nano-filler-polymer interface can significantly affect the transport properties of the composite material [124,127]. The transport properties of the polymer nanocomposite membrane depend on the nature of the nano-filler distribution in the polymer matrix and the interaction between the filler and the matrix along the interphase boundary [145]. Therefore, an improvement in the permeability and selectivity of the nanocomposite membrane as compared to the reinforced polymeric membrane can be associated with an additional volume at the interface or with free volume arising as a result of disruption of polymer chain packing [1,146].

The Maxwell equation was successfully used to predict the permeability of some MMMs with microsize particles. The shape and size of the particles were not taken into account, as was the exponential growth of the permeability of polymer membranes with nanoparticles [130].

Despite the attempts to predict the transport properties presented above, the effective design of nanocomposite membranes such as filled polymer films is impeded by the lack of a fundamental understanding of the effect of nano-fillers on the penetrating diffusion in nanoparticle-polymer composite (NP-PC) membranes. Studying membranes of NP-PC type, Merkel et al. focused their efforts on understanding the three factors that they considered to be the most important for understanding the transport of liquids or gases: The level of loading of nanoparticles, the interaction of nanoparticles, and the distance from the surface of the particle above which the matrix material is perturbed (i.e., has an increased penetrating diffusion) [127,128]. This approach is similar to those presented above and is suggested for the study of MMM.

Efforts have been made to influence the nature and course of this interface processes in two ways: By choosing a matrix polymer with certain functional groups [121] and surface modification of particles [37,123].

From this position, it is necessary to take into account that the effects brought by nanoparticles in transport (in particular, barrier) characteristics of MMM depend primarily on the surface properties of these nano-fillers. It is generally believed that the cause of the anomalous behavior observed for nano-scale particles is a large specific interphase region compared to micron or larger fillers, taking into account the same loading level. When the volume fraction of particles is added to the polymer, a specific interphase region is formed. Therefore, in comparison with the introduction of micron-sized particles to highly permeable membranes, leading to an adverse volume effect, the addition of nanoparticles can create a specific interface with an area of a larger order of magnitude and play a positive role. The addition of nanoparticles is a promising approach to controlling the permeability of polymer membranes. A diffusion of gaseous or liquid penetrants in a composite membrane of the filled polymer type, as mentioned earlier, is enhanced by the presence of a thin “skin” of the matrix material near the nanoparticle surface with a penetrant diffusion coefficient 100 times larger than the matrix. The influence of skin thickness, the fraction of the area of nanoparticles, and the method of nanoparticle distribution in the membrane on the diffusion of the penetrating substance was studied in Reference [147].

However, for the PAI nanocomposites under consideration, the water-permeability of PAI-2-SNT, other things being equal, should be lower than the permeability of PAI-1-SNT [112,121]. We have observed in the transition from PAI-1-SNT to PAI-2-SNT an increase in the permeability of polar liquids and a decrease in permeability with cyclohexane. Apparently, the current research of the gas transport properties of the composite films under consideration with respect to CO<sub>2</sub> and CH<sub>4</sub> (selectivity of diffusion) can bring useful information. Perhaps the determining factor is the aspect number of particles introduced, which did not appear at the level of the transition in the SNT-I-III series for PAI-1 composites, but can manifest itself in the transition to nanofibers? The structural and morphological characteristics of nanoparticles, in particular, the presence of functional groups or internal channels in their structure are essential, or not?

We proposed the formation and investigation of a new nanocomposite of the PAI type containing triple chain Na–Mg-hydrosilicates synthesized under the hydrothermal conditions (nanofibers with the ribbon form, SNF). The obtained fibrous Na<sub>2</sub>Mg<sub>4</sub>Si<sub>6</sub>O<sub>16</sub>(OH)<sub>2</sub> hydrosilicate have the structure built of three silicon-oxygen chains. Such nanoparticles significantly differed from the earlier studied nanotubes by other morphology and size; SNF have never been used early to form membrane nanocomposites.

SNF images obtained by SEM are presented in Figure 28. As seen, the prepared nanoparticles were formed of the 0.05–0.2 mm long and 10–100 nm thick fibers arranged in bundles. Besides the triple chain hydrosilicate fibers, admixture of thin needle-like nanoparticles (0.2–0.5 mm long and 10–50 nm thick) was observed, assigned to the double chain Na–Mg hydrosilicate (the richterite amphibole).

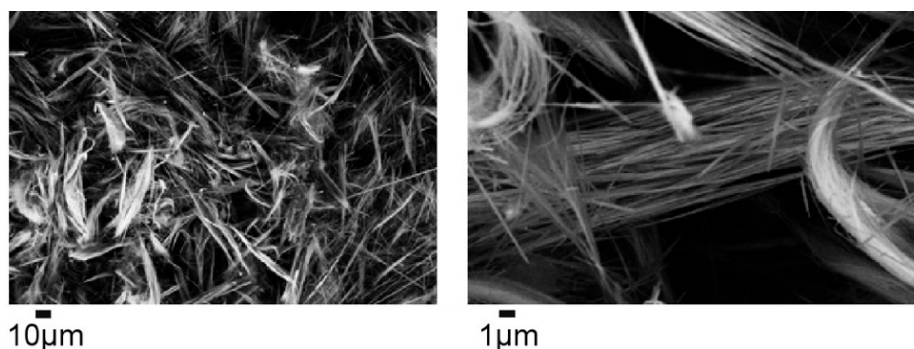
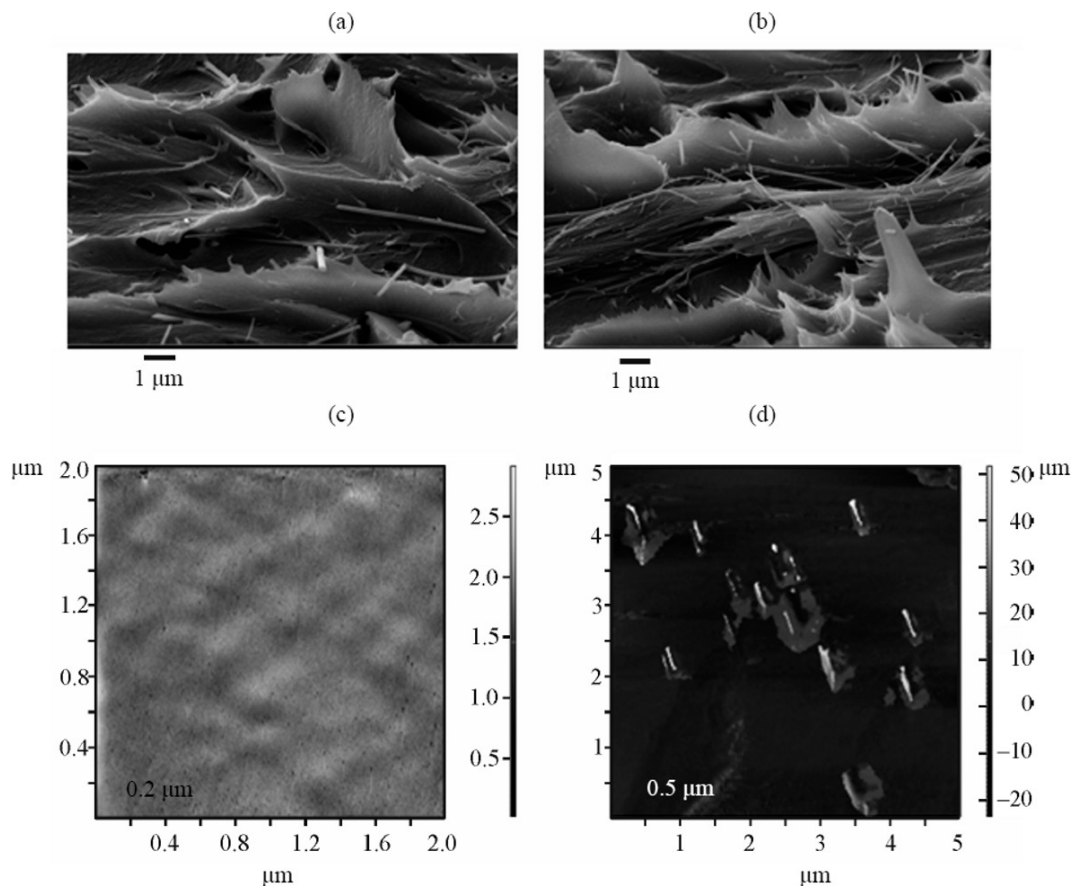


Figure 28. SEM images of Na<sub>2</sub>Mg<sub>4</sub>Si<sub>6</sub>O<sub>16</sub>(OH)<sub>2</sub> hydrosilicate (SNF) [148].

The introduction of these particles led to significant changes in the physical, chemical and thermo-physical properties of the material [142,148], that probably, is in particular due to the increase in the aspect ratio and the planar orientation of SNF in composite film. The morphology (Figure 29), thermo-physical, and relaxation properties of the prepared materials have been studied and analyzed accounting for the nanoparticles structure.



**Figure 29.** Visualization of the film of polyamide-imide composite with triple chain hydrosilicate: (a,b) the cross-section (SEM) and (d) phase contrast AFM; (c) the surface (topography mode AFM) [148].

The introduced SNF disrupts a supramolecular structure of polymer, and the small angle peak observed in the X-ray pattern of the unfilled PAI-1 is thus absent in the X-ray diffractogram of the nanocomposite film. At the same time, the reflexes related to SNF at  $\theta = 9.67$  and  $\theta = 27.7$  are observed, that corresponds to the interplanar distances  $d/n = 9.15$  and  $3.20 \text{ \AA}$ , respectively. It should be mentioned, that the same content of SNT in the PAI-1 does not disrupt the polymer matrix structure, and no reflexes connected with SNT were not registered.

Compared to SNT, introduction of the SNF in PAI-1 film did not lead to increasing of  $T_g$ . But sub-glass transition temperature ( $T_\gamma$ ) connected with free volume (FFV) [148] is more sensitive to nanoparticles introduction, which is very important for gas-separation membranes.

First results of the study of the pervaporation characteristics of PAI-1-SNF showed significant differences in the properties of film samples of PAI-1-SNF and PAI-1-SNT composites, as well as the initial PAI-1 [149].

Pervaporation properties of the formed membranes were studied at  $40 \text{ }^\circ\text{C}$  relative to cyclohexane, ethanol, methanol and water in different sequences of experiments. The data in Figure 30a,b shows that the PAI-1 and PAI-1-SNF films have an equally low permeability of cyclohexane, almost equal to ethanol permeability, and very high permeability for methanol. Interestingly, the introduction of SNFs

into this polymer results in a decrease in methanol permeability and an increase to the permeability of water.

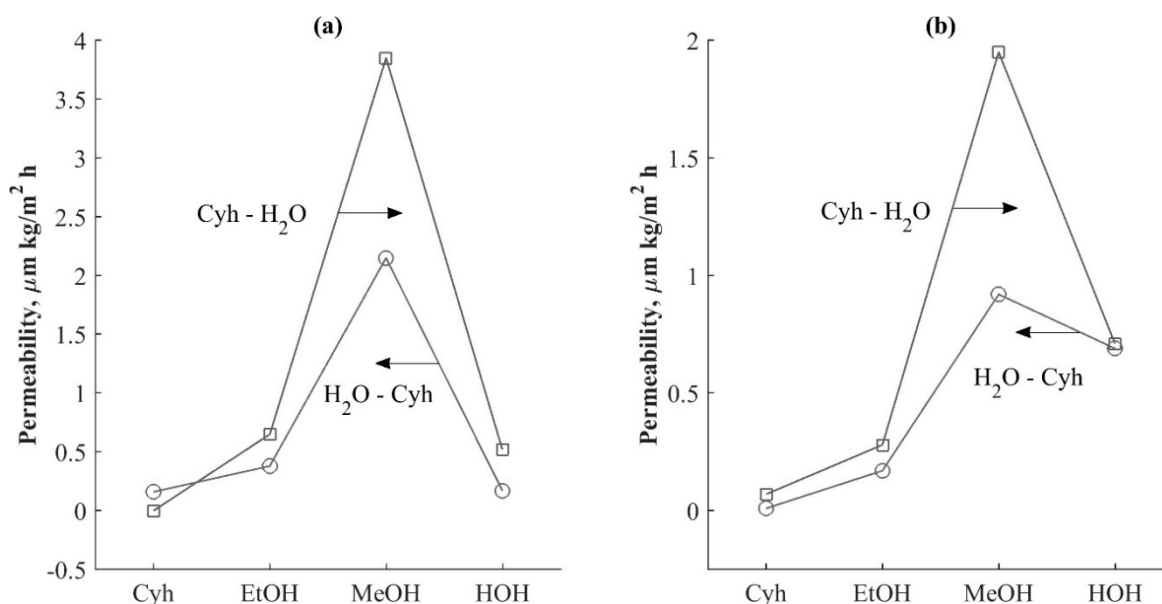


**Figure 30.** Pervaporation properties of (a) PAI-1 and (b) PAI-1-SNF films (Cyh—cyclohexane, EtOH—ethanol, MeOH—methanol, HOH—water). The sequence of penetrants during the pervaporation is as follows: direction 1: Cyh → EtOH → MeOH → HOH; direction 2: HOH → MeOH → EtOH → Cyh [150].

The permeability to cyclohexane substantially reduced during the transition to PAI-1-SNT (the embedding of a low permeable inorganic phase into the unperturbed anisotropic polymer matrix) when inserting the same quantity of the SNF phase, resulting in the formation of the less ordered PAI-1-SNF composite. The permeability to cyclohexane of the PAI-1-SNT film is significantly reduced after its contact with polar solvents under pervaporation conditions due to the removal of excess nano-sized voids, resulting in the formation of a characteristic PAI-1 structure. In the case of water pervaporation, the permeability of PAI-1-SNT is approximately twice as high as in PAI-1, while the permeability of PAI-1-SNF is somewhat reduced. The latter effect is most likely associated with the specific properties of nano-fillers.

We assume that our experiments on the study of the liquid's pervaporation transfer through PAI-1,2-SNF composites, in comparison with PAI-1,2-SNT, will be fruitful to detect key factors affecting transport characteristics of developed materials.

### 3. Conclusions and Future Recommendations

Factual data presented in this review proves once again how complex the systems are, nanocomposites of the type of filled polymers and how the effects of nano-fillers on the transport properties of the corresponding membranes are in some cases unpredictable. However, as a result of the formation of nanocomposites of this type, unique membrane characteristics can be achieved. This applies both to porous and to continuous polymer composites containing nano-fillers. Great prospects in this field of membrane science are associated with the appearance of special techniques for the inclusion of nanoparticles in the material [43,52,151], with the expansion of the spectrum of nano-fillers from which a useful effect is expected [45,52,148,152,153], as well as with the appearance of methods for analyzing and visualizing the distribution and the state of fillers in matrices of different morphologies [29,51,135,154]. New polymeric materials are engaged in the synthesis of nanocomposite membranes, including those responsive to stimuli, and are also capable of self-organization or forming

compositionally heterogeneous films [92,97,102,155–157]. Their use makes it possible to influence the nature of the distribution of nano-fillers in the matrix. Composite membranes obtained acquire a new set of properties, in particular, for the pervaporation separation of liquids, as illustrated above, as well as in a number of review papers [158,159].

An analysis of the results presented in the review shows that all cases under consideration can be classified into three categories for which properties of composite materials are determined by:

- (1) characteristics of nanoparticles introduced into the polymer matrix—their functional, dimensionality, quantity and distribution pattern in a polymer medium;
- (2) effects of nano-fillers on the polymer, which lead to a change in its supramolecular organization, in particular, to the formation of films whose structural-morphological properties differ significantly from those characteristic of the original polymer itself;
- (3) characteristics of the region at the boundary of the inorganic and polymer phases. It is in this area of the composite where each of the components manifests itself as a participant in most processes, and that its functional groups may have a different reactive capacity under specific spatial conditions, in particular under conditions of limited movement of molecules or fragments thereof. In this connection, the question arises of the role of interaction between the polymer and inorganic phases, the adhesion and formation of nano- or larger-sized voids.

Only an integrated approach and consideration of all three of these situations can lead to the development of an algorithm for the directed change in the properties of membrane materials, taking into account a special separation problem. Methods of studying in the variant “from the opposite”, as well as the methods of gradual elimination of individual factors of influence can be used for the investigation of such systems, which are not easily accessible for analysis by direct analytical methods. Such methods include the technique of alternative choice that we have illustrated in our works with an alternative choice of a polymer matrix or nanoparticles, other things being equal. The work in this direction is expected to be promising for determination of base factors of the influence on transport properties, especially in combination with the experimental attempts to change the conditions for the introduction of nanoparticles into a polymer film (simple mixing of components, their mixing with additional external action, introduction of particles at the stage of polymer synthesis in reaction medium, etc.).

**Conflicts of Interest:** The authors declare no conflict of interest.

## References

1. Paul, D.R.; Robeson, L.M. Polymer nanotechnology. Nanocomposites. *Polymer* **2008**, *49*, 3187–3204. [[CrossRef](#)]
2. Sreekumar, T.V.; Liu, T.; Min, B.G.; Guo, H.; Kumar, S.; Hauge, R.H.; Smalley, R.E. Polyacrylonitrile single-walled carbon nanotube composite fibers. *Adv. Mater.* **2004**, *16*, 58–61. [[CrossRef](#)]
3. Figovsky, O.; Beilin, D. *Advanced Polymer Concretes and Compounds*, 1st ed.; Taylor & Francis Group, CRC Press: Boca Roca, FL, USA, 2013.
4. Yudin, V.E.; Otaigbe, J.U.; Gladchenko, S.V.; Olson, B.G.; Nazarenko, S.; Korytkova, E.N.; Gusarov, V.V. New polyimide nanocomposites based on silicate type nanotubes: Dispersion, processing and properties. *Polymer* **2007**, *48*, 1306–1315. [[CrossRef](#)]
5. Hussain, F.; Hojjati, M.; Okamoto, M.; Gorga, R.E. Review article: Polymer-matrix nanocomposites, processing, manufacturing, and application: An overview. *J. Compos. Mater.* **2006**, *40*, 1511–1575. [[CrossRef](#)]
6. Ober, C.K.; Cheng, S.Z.D.; Hammond, P.T.; Muthukumar, M.; Reichmanis, E.; Wooley, K.L.; Lodge, T.P. Research in Macromolecular Science: Challenges and Opportunities for the Next Decade. Perspective. *Macromolecules* **2009**, *42*, 465–471. [[CrossRef](#)]
7. Mai, Y.W.; Yu, Z.Z. *Polymer Nanocomposites*; CRC Press: Boca Raton, FL, USA; Boston, MA, USA; New York, NY, USA; Washington, DC, USA, 2006; p. 594.

8. Tjong, S.C. Structural and mechanical properties of polymer nanocomposites. *Mater. Sci. Eng. R. Rep.* **2006**, *53*, 73–197. [[CrossRef](#)]
9. Spitalsky, Z.; Tasis, D.; Papagelis, K.; Galiotis, C. Carbon nanotube–polymer composites: Chemistry, processing, mechanical and electrical properties. *Prog. Polym. Sci.* **2010**, *35*, 357–401. [[CrossRef](#)]
10. Mondal, S. Polymer Nano-Composite Membranes. *J. Membr. Sci. Technol.* **2015**, *5*, 134–135. [[CrossRef](#)]
11. Yudin, V.E.; Svetlichnyi, V.M. Effect of the structure and shape of filler nanoparticles on the physical properties of polyimide composites. *Russ. J. Gen. Chem.* **2010**, *80*, 2157–2169. [[CrossRef](#)]
12. Gofman, I.V.; Ivan'kova, E.M.; Abalov, I.V.; Smirnova, V.E.; Popova, E.N.; Yudin, V.E.; Orell, O.; Vuorinen, J. Effect of nanoparticles of various types as fillers on mechanical properties of block samples of a heat-resistant polyimide material: A comparative analysis. *Polym. Sci. Ser. A* **2016**, *58*, 87–94. [[CrossRef](#)]
13. Ray, S.S.; Okamoto, M. Polymer/layered silicate nanocomposites: A review from preparation to processing. *Prog. Polym. Sci.* **2003**, *28*, 1539–1641. [[CrossRef](#)]
14. Zeng, Q.; Yu, A.; Lu, G.; Paul, D. Clay-based polymer nanocomposites: Research and commercial development. *J. Nanosci. Nanotechnol.* **2005**, *5*, 1574–1592. [[CrossRef](#)] [[PubMed](#)]
15. Yudin, V.E.; Otaigbe, J.U.; Svetlichnyi, V.M.; Korytkova, E.N.; Almjashaeva, O.V.; Gusarov, V.V. Effects of nano-filler morphology and aspect ratio on the rheo-mechanical properties of polyimide nanocomposites. *Express Polym. Lett.* **2008**, *2*, 485–493. [[CrossRef](#)]
16. Golubeva, O.Y.; Yudin, V.E.; Didenko, A.L.; Svetlichnyi, V.M.; Gusarov, V.V. Nanocomposites based on polyimide thermoplastics and magnesium silicate nanoparticles with montmorillonite structure. *Russ. J. Appl. Chem.* **2007**, *80*, 106–109. [[CrossRef](#)]
17. Gofman, I.V.; Svetlichnyi, V.M.; Yudin, V.E.; Dobrodumov, A.V.; Didenko, A.L.; Abalov, I.V.; Korytkova, E.N.; Egorov, A.I.; Gusarov, V.V. Modification of films of heat-resistant polyimides by adding hydrosilicate and carbon nanoparticles of various geometries. *Russ. J. Gen. Chem.* **2007**, *77*, 1158–1163. [[CrossRef](#)]
18. Yudin, V.E.; Otaigbe, J.U.; Nazarenko, S.I.; Kim, W.D.; Korytkova, E.N. A comparative study on the mechanical and barrier characteristics of polyimide nanocomposite films filled with nanoparticles of planar and tubular morphology. *Mech. Compos. Mater.* **2011**, *47*, 335–342. [[CrossRef](#)]
19. Mulder, M. *Basic Principles of Membrane Technology*, 2nd ed.; Kluwer Academic: Dordrecht, The Netherlands, 1996.
20. Mittal, V. Mechanical and Gas Barrier Properties of Polypropylene Layered Silicate Nanocomposites: A Review. *Open Macromol. J.* **2012**, *6*, 37–52. [[CrossRef](#)]
21. Nunes, S.P.; Schultz, J.; Peinemann, K.V. Silicone membranes with silica nanoparticles. *J. Mater. Sci. Lett.* **1996**, *15*, 1139–1141. [[CrossRef](#)]
22. Nunes, S.P.; Peinemann, K.V.; Ohlrogge, K.; Alpers, A.; Keller, M.; Pires, A.T.N. Membranes of poly(ether imide) and nanodispersed silica. *J. Membr. Sci.* **1999**, *157*, 219–226. [[CrossRef](#)]
23. Chen, B.; Evans, J.R.G. Preferential intercalation in polymer–clay nanocomposites. *J. Phys. Chem. B* **2004**, *108*, 14986–14990. [[CrossRef](#)]
24. Dechnik, J.; Sumbly, C.J.; Janiak, C. Enhancing Mixed-Matrix Membrane Performance with Metal–Organic Framework Additives. *Cryst. Growth Des.* **2017**, *17*, 4467–4488. [[CrossRef](#)]
25. Aroon, M.A.; Ismail, A.F.; Matsuura, T.; Montazer-Rahmati, M.M. Performance studies of mixed matrix membranes for gas separation: A review. *Sep. Purif. Technol.* **2010**, *75*, 229–242. [[CrossRef](#)]
26. Mahajan, R.; Koros, W.J. Mixed matrix materials with glassy polymers. Part 1. *Polym. Eng. Sci.* **2002**, *42*, 1420–1431. [[CrossRef](#)]
27. Koros, W.J.; Mahajan, R. Mixed matrix membrane materials with glassy polymers. Part 2. *Polym. Eng. Sci.* **2002**, *42*, 1432–1441. [[CrossRef](#)]
28. Ismail, A.F.; Norida, R.; Sunarti, A.R. Latest Development on the Membrane Formation for Gas Separation. *Songklanakarin J. Sci. Technol.* **2002**, *24*, 1025–1043.
29. Kononova, S.V.; Gubanova, G.N.; Romashkova, K.A.; Korytkova, E.N.; Timpu, D. Poly (amide-imide) membranes of various morphology: The features of the nano-scale elements of the structure (Book2). In *Atomic Force Microscopy*; Nalladega, V., Ed.; InTech: Rijeka, Croatia, 2012; pp. 81–102.
30. Jhaveri, J.H.; Murthy, Z.V.P. Nanocomposite membranes. *Desalination Water Treat.* **2015**, 1–17. [[CrossRef](#)]
31. Zhang, C.; Dai, Y.; Johnson, J.R.; Karvan, O.; Koros, W.J. High performance ZIF-8/6FDA-DAM mixed matrix membrane for propylene/propane separations. *J. Membr. Sci.* **2012**, *389*, 34–42. [[CrossRef](#)]

32. Jamil, A.; Ching, O.P.; Shariff, A.B.M. Polymer-nanoclay mixed matrix membranes for CO<sub>2</sub>/CH<sub>4</sub> separation: A Review. *Appl. Mech. Mater.* **2014**, *625*, 690–695. [[CrossRef](#)]
33. Souza, V.C.; Quadri, M.G.N. Organic-inorganic hybrid membranes in separation processes: A 10-year review. *Braz. J. Chem. Eng.* **2013**, *30*, 683–700. [[CrossRef](#)]
34. Sun, W.; Shi, J.; Chen, C.; Li, N.; Xu, Z.; Li, J.; Lv, H.; Qian, X.; Zhao, L. A review on organic-inorganic hybrid nanocomposite membranes: A versatile tool to overcome the barriers of forward osmosis. *RSC Adv.* **2018**, *8*, 10040–10056. [[CrossRef](#)]
35. Mushardt, H.; Müller, M.; Shishatskiy, S.; Wind, J.; Brinkmann, T. Detailed investigation of separation performance of a MMM for removal of higher hydrocarbons under varying operating conditions. *Membranes* **2016**, *6*, 16. [[CrossRef](#)] [[PubMed](#)]
36. Lakhotiaa, S.R.; Mukhopadhyay, M.; Kumari, P. A short review: Surface modified nanocomposite membrane. *Sep. Purif. Rev.* **2017**. [[CrossRef](#)]
37. Tal'roze, R.V.; Shandryuk, G.A.; Merekalov, A.S.; Shatalova, A.M.; Otmakhova, O.A. Alignment of nanoparticles in polymer matrices. *Polym. Sci. Ser. A* **2009**, *51*, 1194–1203. [[CrossRef](#)]
38. Ozdemir, S.S.; Buonomenna, M.G.; Drioli, E. Catalytic polymeric membranes: Preparation and application. Review. *Appl. Catal. A Gen.* **2006**, *307*, 167–183. [[CrossRef](#)]
39. Kim, D.J.; Jo, M.J.; Nam, S.Y. A review of polymer-nanocomposite electrolyte membranes for fuel cell application. *J. Ind. Eng. Chem.* **2015**, *21*, 36–52. [[CrossRef](#)]
40. Qadir, D.; Mukhtar, H.; Keong, L.K. Mixed matrix membranes for water purification applications. A Review. *J. Sep. Purif. Rev.* **2017**, *46*, 62–80. [[CrossRef](#)]
41. Pendergast, M.T.M.; Hoek, E.M.V. A review of water treatment membrane nanotechnologies. *Energy Environ. Sci.* **2011**, *4*, 1946–1971. [[CrossRef](#)]
42. Tjink, M.S.L.; Kooman, J.; Wester, M.; Sun, J.; Saiful, S.; Joles, J.A.; Borneman, Z.; Wessling, M.; Stamatialis, D.F. Mixed Matrix Membranes: A new asset for blood purification therapies. *Blood Purif.* **2014**, *37*, 1–3. [[CrossRef](#)] [[PubMed](#)]
43. Dotzauer, D.M.; Dai, J.; Sun, L.; Bruening, M.L. Catalytic membranes prepared using layer-by-layer adsorption of polyelectrolyte/metal nanoparticle films in porous supports. *Nano Lett.* **2006**, *6*, 2268–2272. [[CrossRef](#)] [[PubMed](#)]
44. Zhong, J.; Wen, W.Y.; Jones, A.A. Enhancement of diffusion in a high-permeability polymer by the addition of nanoparticles. *Macromolecules* **2003**, *36*, 6430–6432. [[CrossRef](#)]
45. Janakiram, S.; Ahmadi, M.; Dai, Z.; Ansaloni, L.; Deng, L. Performance of nanocomposite membranes containing 0D to 2D nano-fillers for CO<sub>2</sub> separation: A review. *Membranes* **2018**, *8*, 24. [[CrossRef](#)] [[PubMed](#)]
46. Khan, M.M.; Filiz, V.; Bengtson, G.; Shishatskiy, S.; Rahman, M.; Abetz, V. Functionalized carbon nanotubes mixed matrix membranes of polymers of intrinsic microporosity for gas separation. *Nanoscale Res. Lett.* **2012**, *7*, 504. [[CrossRef](#)] [[PubMed](#)]
47. Weigelt, F.; Georgopoulos, P.; Shishatskiy, S.; Filiz, V.; Brinkmann, T.; Abetz, V. Development and characterization of defect-free Matrimid<sup>®</sup> mixed-matrix membranes containing activated carbon particles for gas separation. *Polymers* **2018**, *10*, 51. [[CrossRef](#)]
48. Van der Bruggen, B. The separation power of nanotubes in membranes: A Review. *Nanotechnology* **2012**, 693485. [[CrossRef](#)]
49. Jia, M.; Peinemann, K.V.; Behling, R.D. Molecular sieving effect of the zeolite-filled silicone rubber membranes in gas permeation. *J. Membr. Sci.* **1991**, *57*, 289–296. [[CrossRef](#)]
50. Suer, M.G.; Bac, N.; Yilmaz, L. Gas permeation characteristics of polymer-zeolite mixed matrix membranes. *J. Membr. Sci.* **1994**, *91*, 77–86. [[CrossRef](#)]
51. Richards, H.L.; Baker, P.G.L.; Iwuoha, E. Metal nanoparticle modified polysulfone membranes for use in wastewater treatment: A Critical Review. *J. Surf. Eng. Mater. Adv. Technol.* **2012**, *2*, 183–193. [[CrossRef](#)]
52. Zhao, W.; Huang, J.; Fang, B.; Nie, S.; Yi, N.; Su, B.; Li, H.; Zhao, C. Modification of polyethersulfone membrane by blending semi-interpenetrating network polymeric nanoparticles. *J. Membr. Sci.* **2011**, *369*, 258–266. [[CrossRef](#)]
53. Jiang, L.Y.; Chung, T.-S.; Rajagopalan, R. Matrimid/MgO mixed matrix membranes for pervaporation. *AIChE J.* **2007**, *53*, 1745–1757. [[CrossRef](#)]

54. Upadhyaya, L.; Semsarilar, M.; Nehache, S.; Cot, D.; Fernández-Pacheco, R.; Martinez, G.M.; Mallada, R.; Deratani, A.; Quemener, D. Nanostructured mixed matrix membranes from supramolecular assembly of block copolymer nanoparticles and iron oxide nanoparticles. *Macromolecules* **2016**, *49*, 20. [[CrossRef](#)]
55. Goh, P.S.; Ismail, A.F. Review: Is interplay between nanomaterial and membrane technology the way forward for desalination? *J. Chem. Technol. Biotechnol.* **2015**, *90*, 971–980. [[CrossRef](#)]
56. Goh, P.S.; Matsuura, T.; Ismail, A.F.; Hilal, N. Recent trends in membranes and membrane processes for desalination. *Desalination* **2016**, *391*, 43–60. [[CrossRef](#)]
57. Freeman, B. Basis of permeability/selectivity tradeoff relations in polymeric gas separation membranes. *Macromolecules* **1999**, *32*, 375–380. [[CrossRef](#)]
58. Sholl, D.S.; Johnson, J.K. Making high-flux membranes with carbon nanotubes. *Science* **2006**, *312*, 1003–1004. [[CrossRef](#)] [[PubMed](#)]
59. Yang, Y.; Zhang, H.; Wang, P.; Zheng, Q.; Li, J. The influence of nano-sized TiO<sub>2</sub> fillers on the morphologies and properties of PSFUF membrane. *J. Membr. Sci.* **2007**, *288*, 231–238. [[CrossRef](#)]
60. Liu, L.; Jiang, Z.; Pan, F.; Peng, F.; Wu, H. The unusual change of permeation rate in PDMS membranes filled with crystalline calixarene and its derivative. *J. Membr. Sci.* **2006**, *279*, 111–119. [[CrossRef](#)]
61. Lu, L.; Sun, H.; Peng, F.; Jiang, Z.Y. Novel graphite-filled PVA/CS hybrid membranes for pervaporation of benzene/cyclohexane mixture. *J. Membr. Sci.* **2006**, *281*, 245–252. [[CrossRef](#)]
62. Goedel, W.A. A simple theory of particle-assisted wetting. *Europhys. Lett.* **2003**, *62*, 607–613. [[CrossRef](#)]
63. Xu, H.; Goedel, W. Polymer–Silica Hybrid Monolayers as Precursors for Ultrathin Free-Standing Porous Membranes. *Langmuir* **2002**, *18*, 2363–2367. [[CrossRef](#)]
64. Xu, H.; Goedel, W. From particle-assisted wetting to thin free-standing porous membranes. *Angew. Chem. Int. Ed.* **2003**, *42*, 4694–4696. [[CrossRef](#)] [[PubMed](#)]
65. Choi, J.H.; Jegal, J.; Kim, W.N. Fabrication and characterization of multi-walled carbon nanotubes/polymer blend membranes. *J. Membr. Sci.* **2006**, *284*, 406–415. [[CrossRef](#)]
66. Cornelius, C.J.; Marand, E. Hybrid silica–polyimide composite membranes: Gas transport properties. *J. Membr. Sci.* **2002**, *202*, 97–118. [[CrossRef](#)]
67. Joly, C.; Goizet, S.; Schrotter, J.C.; Sanchez, J.; Escoubes, M. Sol–gel polyimide–silica composite membrane: Gas transport properties. *J. Membr. Sci.* **1997**, *130*, 63–74. [[CrossRef](#)]
68. Hu, Q.; Marand, E.; Dhingra, S.; Fritsch, D.; Wen, J.; Wilkes, G. Poly(amide–imide)/TiO<sub>2</sub> nano-composite gas separation membranes: Fabrication and characterization. *J. Membr. Sci.* **1997**, *135*, 65–79. [[CrossRef](#)]
69. Park, H.B.; Kim, J.K.; Nam, S.Y.; Suresh, A.K.; Bellare, J.; Sridhar, T.; Wang, H. Imide–siloxane block copolymer/silica hybrid membranes: Preparation, characterization and gas separation properties. *J. Membr. Sci.* **2003**, *220*, 59–73. [[CrossRef](#)]
70. Hamciuc, C.; Hamciuc, E.; Vlad-Bubulac, T.; Vlad, S.; Asandulesa, M.; Wolinska-Grabczyk, A. Silica-containing polyetherimide hybrid films based on methyltriethoxysilane as precursor of inorganic network. *Polym. Test.* **2016**, *52*, 94–103. [[CrossRef](#)]
71. Wahab, M.F.A.; Rahim, R.A.; Ismail, A.F. Latest development of mixed matrix membrane using glassy polymer as continuous phase for gas separation. In Proceedings of the Regional Symposium on Membrane Science and Technology, Puteri Pan Pacific Hotel, Johor Bahru, Malaysia, 21–25 April 2004.
72. Funk, C.V.; Lloyd, D.R. Zeolite-filled microporous mixed matrix (ZeoTIPS) membranes: Prediction of gas separation performance. *J. Membr. Sci.* **2008**, *313*, 224–231. [[CrossRef](#)]
73. Mahajan, R.; Koros, W.J. Factors controlling successful formation of mixed-matrix gas separation materials. *Ind. Eng. Chem. Res.* **2000**, *39*, 2692–2696. [[CrossRef](#)]
74. Zimmerman, C.M.; Singh, A.; Koros, W.J. Tailoring mixed matrix composite membrane for gas separations. *J. Membr. Sci.* **1997**, *137*, 145–154. [[CrossRef](#)]
75. Mahajan, R. Formation, Characterization and Modeling of Mixed Matrix Membrane Materials. Ph.D. Thesis, The University of Texas at Austin, Austin, TX, USA, 2000.
76. Tantekin-Ersolmaz, S.B.; Senorkyan, L.; Kalaonra, N.; Tatlier, M.; Erdem-Sen-atar, A. n-pentane/i-pentane separation by using zeolite–PDMS mixed matrix membranes. *J. Membr. Sci.* **2001**, *189*, 59–67. [[CrossRef](#)]
77. Vu, D.Q.; Koros, W.J.; Miller, S.J. Mixed matrix membranes using carbon molecular sieves I. Preparation and experimental result. *J. Membr. Sci.* **2003**, *211*, 311–334. [[CrossRef](#)]

78. Ferraris, J.P.; Musselman, I.H.; Balkus, K.J. Mixed matrix membranes based on metal organic frameworks. In *Advanced Materials for Membrane Preparation*; Bentham Science Publishers: Sharjah, UAE, 2012; Volume 11, pp. 83–93, ISBN 978-1-60805-505-0. [[CrossRef](#)]
79. Robeson, L.M. Correlation of separation factor versus permeability for polymeric membranes. *J. Membr. Sci.* **1991**, *62*, 165–185. [[CrossRef](#)]
80. Robeson, L.M. The Upper bound revisited. *J. Membr. Sci.* **2008**, *320*, 390–400. [[CrossRef](#)]
81. Vu, D.Q. Formation and Characterization of Asymmetric Carbon Molecular Sieve and Mixed Matrix Membranes for Natural Gas Purification. Ph.D. Thesis, The University of Texas at Austin, Austin, TX, USA, 2001.
82. Gorgojo, P.; de la Iglesia, O.; Coronas, J. Preparation and characterization of zeolite membranes. *Membr. Sci. Technol.* **2008**, *13*, 135–175. [[CrossRef](#)]
83. Favvas, E.P.; Katsaros, F.K.; Papageorgiou, S.K.; Sapalidis, A.A.A.; Mitropoulos, C. A review of the latest development of polyimide based membranes for CO<sub>2</sub> separations. *React. Funct. Polym.* **2017**, *120*, 104–130. [[CrossRef](#)]
84. Goh, P.S.; Ismail, A.F.; Sanip, S.M.; Ng, B.C.; Aziz, M. Recent advances of inorganic fillers in mixed matrix membrane for gas separation. *Sep. Purif. Technol.* **2011**, *81*, 243–264. [[CrossRef](#)]
85. Duval, J.M.; Folkers, B.; Mulder, M.H.V.; Desgrandchamps, G.; Smolders, C.A. Adsorbent filled membranes for gas separation. Part 1. Improvement of the gas separation properties of polymeric membranes by incorporation of microporous adsorbents. *J. Membr. Sci.* **1993**, *80*, 189–198. [[CrossRef](#)]
86. Yong, H.H.; Park, H.C.; Kang, Y.S.; Won, J.; Kim, W.N. Zeolite-filled polyimide membrane containing 2,4,6-triaminopyrimidine. *J. Membr. Sci.* **2001**, *188*, 151–163. [[CrossRef](#)]
87. Mahajan, R.; Burns, R.; Schaeffer, M.; Koros, W.J. Challenges in forming successful mixed matrix membranes with rigid polymeric materials. *J. Appl. Polym. Sci.* **2002**, *86*, 881–890. [[CrossRef](#)]
88. Gao, Z.; Yue, Y.; Li, W. Application of zeolite-filled pervaporation membrane. *Zeolites* **1996**, *16*, 70–74. [[CrossRef](#)]
89. Zhang, Y.; Balkus, K.J., Jr.; Musselman, I.H.; Ferraris, J.P. Mixed-matrix membranes composed of Matrimid® and mesoporous ZSM-5 nanoparticles. *J. Membr. Sci.* **2008**, *325*, 28–39. [[CrossRef](#)]
90. Hamciuc, E.; Hamciuc, C.; Musteata, V.E.; Kalvachev, Y.; Wolinska-Grabczyk, A. Preparation and characterization of new polyimide films containing zeolite L and/or silica. *High Perform. Polym.* **2014**, *26*, 175–187. [[CrossRef](#)]
91. Suzuki, T.; Yamada, Y.; Sakai, J. Gas transport properties of ODP-PA-TAPOB hyperbranched polyimide–silica hybrid membranes. *High Perform. Polym.* **2006**, *18*, 655–664. [[CrossRef](#)]
92. Suzuki, T.; Yamada, Y. Characterization of 6FDA-based hyperbranched and linear polyimide–silica hybrid membranes by gas permeation and <sup>129</sup>Xe NMR measurements. *J. Polym. Sci. Part B Polym. Phys.* **2006**, *44*, 291–298. [[CrossRef](#)]
93. Cong, H.; Radosz, M.; Towler, B.F.; Shen, Y. Review: Polymer–inorganic nanocomposite membranes for gas separation. *Sep. Purif. Technol.* **2007**, *55*, 281–291. [[CrossRef](#)]
94. Breck, D.W. *Zeolite Molecular Sieves*; John Wiley & Son: New York, NY, USA, 1974.
95. Yang, R.T. *Gas Separation by Adsorption Process*; Imperial College Press: London, UK, 1997.
96. Ji, W.; Sikdar, S.K. Pervaporation using adsorbent-filled membranes. *Ind. Eng. Chem. Res.* **1996**, *35*, 1124–1132. [[CrossRef](#)]
97. Savage, N.; Diallo, M.S. Nanomaterials and water purification: Opportunities and challenges. *J. Nanopart. Res.* **2005**, *7*, 331–342. [[CrossRef](#)]
98. Sokhan, V.P.; Nicholson, D.; Quirke, N. Fluid flow in nanopores: Accurate boundary conditions for carbon nanotubes. *J. Chem. Phys.* **2002**, *117*, 8531–8539. [[CrossRef](#)]
99. Hinds, B.J.; Chopra, N.; Rantell, T.; Andrews, R.; Galvalas, V.; Bachas, L.G. Aligned multiwalled carbon nanotube membranes. *Science* **2004**, *303*, 62–65. [[CrossRef](#)] [[PubMed](#)]
100. Majumder, M.; Chopra, N.; Andrews, R.; Hinds, B.J. Nanoscale hydrodynamics: Enhanced flow in carbon nanotubes. *Nature* **2005**, *438*, 44. [[CrossRef](#)] [[PubMed](#)]
101. Skoulidas, A.I.; Sholl, D.S.; Johnson, J.K. Adsorption and diffusion of carbon dioxide and nitrogen through single-walled carbon nanotube membranes. *J. Chem. Phys.* **2006**, *124*, 054708. [[CrossRef](#)] [[PubMed](#)]

102. Boker, A.; Lin, Y.; Chiapperini, K.; Horowitz, R.; Thompson, M.; Carreon, V.; Xu, T.; Abetz, C.; Skaff, H.; Dinsmore, A.D.; et al. Hierarchical nanoparticle assemblies formed by decorating breath figures. *Nat. Mater.* **2004**, *3*, 302–306. [[CrossRef](#)] [[PubMed](#)]
103. Mark, J.E.; Jiang, C.Y.; Tang, M.Y. Simultaneous curing and filling of elastomers. *Macromolecules* **1984**, *17*, 2613–2616. [[CrossRef](#)]
104. Uddin, F. Clays, Nanoclays, and Montmorillonite Minerals. *Metall. Mater. Trans. A* **2008**, *39*, 2804–2814. [[CrossRef](#)]
105. Fornes, T.D.; Hunter, D.L.; Paul, D.R. Effect of sodium montmorillonite source on nylon 6/clay nanocomposites. *Polymer* **2004**, *45*, 2321–2331. [[CrossRef](#)]
106. Gorrasi, G.; Tortora, M.; Vittoria, V.; Kaempfer, D.; Mulhaupt, R. Vapor barrier properties of polycaprolactone montmorillonite nanocomposites: Effect of clay dispersion. *Polymer* **2003**, *44*, 2271–2279. [[CrossRef](#)]
107. Zeng, Q.H.; Wang, D.Z.; Yu, A.B.; Lu, G.Q. Synthesis of polymer–montmorillonite nanocomposites by in situ intercalative polymerization. *Nanotechnology* **2002**, *13*, 549–553. [[CrossRef](#)]
108. Hasegawa, N.; Okamoto, H.; Kato, M.; Usuki, A.; Saton, N. Nylon 6/Na–montmorillonite nanocomposites prepared by compounding Nylon 6 with Na–montmorillonite slurry. *Polymer* **2003**, *44*, 2933–2937. [[CrossRef](#)]
109. Yano, K.; Usuki, A.; Okada, A.; Toshio, K.; Osami, K. Synthesis and properties of polyimide–clay hybrid. *J. Polym. Sci. Part A Polym. Chem.* **1993**, *31*, 2493–2498. [[CrossRef](#)]
110. Magaraphan, R.; Lilayuthalert, W.; Sirivat, A.; Schwank, J.W. Preparation, structure, properties and thermal behavior of rigid-rod polyimide/montmorillonite nanocomposites. *Compos. Sci. Technol.* **2001**, *61*, 1253–1264. [[CrossRef](#)]
111. Ray, S.S.; Okamoto, K.; Okamoto, M. Structure–property relationship in biodegradable poly(butylene succinate)/layered silicate nanocomposites. *Macromolecules* **2003**, *36*, 2355–2367. [[CrossRef](#)]
112. Kononova, S.V.; Korytkova, E.N.; Romashkova, K.A.; Kuznetsov, Y.P.; Gofman, I.V.; Svetlichnyi, V.M.; Gusarov, V.V. Nanocomposites based on polyamide-imide with hydrosilicate nanoparticle of varied morphology. *Russ. J. Appl. Chem.* **2007**, *80*, 2142–2148. [[CrossRef](#)]
113. Nazarenko, S.; Meneghetti, P.; Julmon, P.; Olson, B.G.; Qutubuddin, S. Gas barrier of polystyrene montmorillonite clay nanocomposites: Effect of mineral layer aggregation. *J. Polym. Sci. Part A Polym. Phys.* **2007**, *45*, 1733–1753. [[CrossRef](#)]
114. Bharadwaj, R.K. Modeling the barrier properties of polymer-layered silicate nanocomposites. *Macromolecules* **2001**, *34*, 9189–9192. [[CrossRef](#)]
115. Nielsen, L.E. Models for the permeability of filled polymer systems. *J. Macromol. Sci. Chem.* **1967**, *5*, 929–942. [[CrossRef](#)]
116. Cussler, E.L.; Hughes, S.E.; Ward, W.J.; Aris, R. Barrier membranes. *J. Membr. Sci.* **1988**, *38*, 161–174. [[CrossRef](#)]
117. Falla, W.R.; Mulski, M.; Cussler, E.L. Estimating diffusion through flake-filled membranes. *J. Membr. Sci.* **1996**, *119*, 129–138. [[CrossRef](#)]
118. Fredrickson, G.H.; Bicerano, J. Barrier properties of oriented disk composites. *J. Chem. Phys.* **1999**, *110*, 2181–2188. [[CrossRef](#)]
119. Chan, S.L. *Image Analysis in Fractography and Failure Mechanisms of Polymers and Composites*; Roulin-Moloney, A.C., Ed.; Elsevier: New York, NY, USA, 1989; p. 145.
120. Adoor, S.G.; Sairam, M.; Manjeshwar, L.S.; Kothapalli, R.V.; Aminabhavi, T.M. Sodium montmorillonite clay loaded novel mixed matrix membranes of poly(vinyl alcohol) for pervaporation dehydration of aqueous mixtures of isopropanol and 1,4-dioxane. *J. Membr. Sci.* **2006**, *285*, 182–195. [[CrossRef](#)]
121. Kononova, S.V.; Korytkova, E.N.; Maslennikova, T.P.; Romashkova, K.A.; Kruchinina, E.V.; Potokin, I.L.; Gusarov, V.V. Polymer-inorganic nanocomposites based on aromatic polyamidoimides effective in the processes of liquids separation. *Russ. J. Gen. Chem.* **2010**, *80*, 1136–1142. [[CrossRef](#)]
122. Hanemann, T.; Szabó, D.V. Review: Polymer-Nanoparticle Composites: From Synthesis to Modern Applications. *Materials* **2010**, *3*, 3468–3517. [[CrossRef](#)]
123. Yudin, V.E.; Bugrov, A.N.; Didenko, A.L.; Smirnova, V.E.; Gofman, I.V.; Kononova, S.V.; Kremnev, R.V.; Popova, E.N.; Svetlichnyi, V.M.; Kudryavtsev, V.V. Composites of multiblock (segmented) aliphatic poly(ester imide) with zirconia nanoparticles: Synthesis, mechanical properties, and pervaporation behavior. *Polym. Sci. Ser. B* **2014**, *56*, 919–926. [[CrossRef](#)]

124. Liang, C.Y.; Uchytel, P.; Petrychkovych, R.; Lai, Y.C.; Lai, Y.-C.; Friess, K.; Sipek, M.; Reddy, M.M.; Suen, S.-Y. Preparation of PES (polyethersulfone)/MMT (Na-montmorillonite) and PES/TiO<sub>2</sub> mixed matrix membranes for CO<sub>2</sub>/CH<sub>4</sub> separation. *Sep. Purif. Technol.* **2012**, *92*, 57–63. [[CrossRef](#)]
125. Merkel, T.C.; Freeman, B.D.; Spontak, R.J.; He, Z.; Pinnau, I.; Meakin, P.; Hill, A.J. Ultraporous reverse-selective nanocomposite membranes. *Science* **2002**, *296*, 519–522. [[CrossRef](#)] [[PubMed](#)]
126. Merkel, T.C.; He, Z.; Pinnau, I.; Freeman, B.D.; Meakin, P.; Hill, A.J. Effect of nanoparticles on gas sorption and transport in poly(1-trimethylsilyl-1-propyne). *Macromolecules* **2003**, *36*, 6844–6855. [[CrossRef](#)]
127. Merkel, T.C.; Freeman, B.D.; Spontak, R.J.; He, Z.; Pinnau, I.; Meakin, P.; Hill, A.J. Sorption, transport, and structural evidence for enhanced free volume in poly(4-methyl-2-pertyne)/fumed silica nanocomposite membranes. *Chem. Mater.* **2003**, *15*, 109–123. [[CrossRef](#)]
128. Merkel, T.C.; Toy, L.G.; Andrady, A.L.; Gracz, H.; Stejskal, E.O. Investigation of enhanced free volume in nanosilica-filled poly(1-trimethylsilyl-1-propyne) by <sup>129</sup>Xe NMR spectroscopy. *Macromolecules* **2003**, *36*, 353–358. [[CrossRef](#)]
129. Stephen, R.; Ranganahaiyah, C.; Varghese, S.; Kim, S.K.; Lee, H.C.; Cho, C.S. Gas transport through nano and micro composites of natural rubber (NR) and their blends with carboxylated styrene butadiene rubber (XSBR) latex membranes. *Polymer* **2006**, *47*, 858–870. [[CrossRef](#)]
130. Wu, Y.; Yudin, V.E.; Otaigbe, J.U.; Korytkova, E.N.; Nazarenko, S. Gas barrier behavior of polyimide films filled with synthetic chrysotile nanotubes. *J. Polym. Sci. Part B Polym. Phys.* **2013**, *51*, 1184–1193. [[CrossRef](#)]
131. Yano, K.; Usuki, A.; Okada, A. Synthesis and properties of polyimide-clay hybrid films. *J. Polym. Sci. Part A Polym. Chem.* **1997**, *35*, 2289–2294. [[CrossRef](#)]
132. Bharadwaj, R.K.; Mehrabi, A.R.; Hamilton, C.; Trujillo, C.; Murga, M.; Fan, R.; Chavira, A.; Thompson, A.K. Structure-property relationships in cross-linked polyester-clay nanocomposites. *Polymer* **2002**, *43*, 3699–3705. [[CrossRef](#)]
133. Maji, P.K.; Das, N.K.; Bhowmick, A.K. Preparation and properties of polyurethane nanocomposites of novel architecture as advanced barrier materials. *Polymer* **2010**, *51*, 1100–1110. [[CrossRef](#)]
134. Gain, O.; Espuche, E.; Pollet, E.; Alexandre, M.; Dubois, P. Gas barrier properties of poly( $\epsilon$ -caprolactone)/clay nanocomposites: Influence of the morphology and polymer/clay interactions. *J. Polym. Sci. Part B Polym. Phys.* **2004**, *43*, 205–214. [[CrossRef](#)]
135. Piperno, S.; Kaplan-Ashiri, I.; Cohen, S.R.; Popovitz-Biro, R.; Wagner, H.D.; Tenne, R.; Foresti, E.; Lesci, I.G.; Roveri, N. Characterization of geoinspired and synthetic chrysotile nanotubes by Atomic Force Microscopy and Transmission Electron Microscopy. *Adv. Funct. Mater.* **2007**, *17*, 3332–3338. [[CrossRef](#)]
136. Livi, K.J.T.; Veblen, D.R. “Eastonite” from Easton, Pennsylvania: A mixture of phlogopite and a new form of serpentine. *Am. Mineral.* **1987**, *72*, 113–125.
137. Korytkova, E.N.; Maslov, A.V.; Gusarov, V.V. *Coll. of Works Surface Chemistry and Synthesis of Low-Dimension Systems*; RIO SPbGTI (TU): St. Petersburg, Russia, 2002; pp. 54–59.
138. Korytkova, E.N.; Maslov, A.V.; Pivovarova, L.N.; Maslennikova, T.P.; Pivovarova, L.N.; Korytkova, E.N. Formation of Mg<sub>3</sub>Si<sub>2</sub>O<sub>5</sub>(OH)<sub>4</sub> nanotubes under hydrothermal conditions. *Glass Phys. Chem.* **2004**, *30*, 72–78. [[CrossRef](#)]
139. Gubanov, G.N.; Kononova, S.V.; Vylegzhanina, M.E.; Sukhanova, T.E.; Grigor’ev, A.I.; Romashkova, K.A.; Svetlichnyi, V.M.; Korytkova, E.N.; Christi, M.; Timpu, D.; et al. Structure, morphology, and thermal properties of nanocomposites based on polyamide-imide and hydrosilicate nanotubes. *Russ. J. Appl. Chem.* **2010**, *83*, 2175–2181. [[CrossRef](#)]
140. Timpu, D.; Gubanov, G.N.; Kononova, S.V. High temperature polyamide imides-hydrosilicates nanocomposites: Structural and morphological aspects. In Proceedings of the 2th International Multidisciplinary Microscopy and Microanalysis Conference—INTERM, Oludeniz-Fethiye-Mugla, Turkey, 16–19 October 2014.
141. Afanas’eva, N.V.; Gubanov, G.N.; Romashkova, K.A.; Sapegin, D.A.; Kononova, S.V. Relaxation processes in an aromatic polyamide-imide and composites on its basis with hydrosilicate nanoparticles. *Polym. Sci. Ser. A* **2016**, *58*, 956–967. [[CrossRef](#)]
142. Gubanov, G.; Kononova, S.; Bronnikov, S. Nanocomposites based on aromatic polyamide-imide and magnesium hydrosilicate nanotubes. *J. Macromol. Sci. B Phys.* **2014**, *53*, 555–567. [[CrossRef](#)]
143. Ma, J.; Zhang, S.; Qi, Z.; Li, G.; Hu, Y. Crystallization behaviors of polypropylene/montmorillonite nanocomposites. *J. Appl. Polym. Sci.* **2002**, *83*, 1978–1985. [[CrossRef](#)]

144. Yudin, V.E.; Feldman, A.Y.; Svetlichnyi, V.M.; Shumakov, A.N.; Marom, G. Crystallization of R-BAPB type polyimide modified by carbon nano-particles. *Compos. Sci. Technol.* **2007**, *67*, 789–794. [[CrossRef](#)]
145. Mondal, S.; Hu, J.L. Microstructure and water vapor transport properties of functionalized carbon nanotube reinforced segmented polyurethane composite membranes. *Polym. Eng. Sci.* **2008**, *48*, 1718–1724. [[CrossRef](#)]
146. Shirazi, Y.; Mohammadi, T. Effects of CNTs content on physicochemical and pervaporation separation properties of PVA membranes. *Sep. Sci. Technol.* **2013**, *48*, 716–727. [[CrossRef](#)]
147. Xue, L.; Borodin, O.; Smith, G.D. Modeling of enhanced penetrant diffusion in nanoparticle-polymer composite membranes. *J. Membr. Sci.* **2006**, *286*, 293–300. [[CrossRef](#)]
148. Gubanova, G.N.; Kononova, S.V.; Cristea, M.; Timpu, D.; Romashkova, K.A.; Korytkova, E.N.; Maslennikova, T.P.; Saprikina, N.N. Morphology and mechanical properties of polymer–inorganic nanocomposite containing triple chain fibrous Na–Mg hydrosilicate. *Russ. J. Gen. Chem.* **2015**, *85*, 1496–1505. [[CrossRef](#)]
149. Kononova, S.V.; Gubanova, G.N.; Kruchinina, E.V.; Maslennikova, T.P.; Pivovarova, L.N.; Korytkova, E.N. Aromatic polyamide-imides modified with hydrosilicate nanoparticles of different structure and morphology for membrane technologies. *Glass Phys. Chem.* **2017**, *43*, 181–184. [[CrossRef](#)]
150. Giwa, A.; Akther, N.; Dufour, V.; Hasan, S.W. A critical review on recent polymeric and nano-enhanced membranes for reverse osmosis process. *RSC Adv.* **2016**, *6*, 8134–8163. [[CrossRef](#)]
151. Gao, P.; Hunter, A.; Benavides, S.; Summe, M.J.; Gao, F.; Phillip, W.A. Template synthesis of nanostructured polymeric membranes by inkjet printing. *ACS Appl. Mater. Interfaces* **2016**, *8*, 3386–3395. [[CrossRef](#)] [[PubMed](#)]
152. Ma, J.; Ping, D.; Dong, X. Recent developments of graphene oxide-based membranes: A Review. *Membranes* **2017**, *7*, 52. [[CrossRef](#)]
153. Orekhov, A.; Klechkovskaya, V.V.; Kononova, S. Low-voltage scanning electron microscopy of multilayer polymer systems. *Crystallogr. Rep.* **2017**, *62*, 710–715. [[CrossRef](#)]
154. Peinemann, K.-V.; Abetz, V.; Simon, P.F.W. Asymmetric superstructure formed in a block copolymer via phase separation. *Nat. Mater.* **2007**, *6*, 992–996. [[CrossRef](#)] [[PubMed](#)]
155. Roy, S.; Singha, N.R. Polymeric nanocomposite membranes for next generation pervaporation process: Strategies, challenges and future prospects. *Membranes* **2017**, *7*, 53. [[CrossRef](#)] [[PubMed](#)]
156. Davey, C.J.; Leak, D.; Patterson, D.A. Hybrid and mixed matrix membranes for separations from fermentations. *Membranes* **2016**, *6*, 17. [[CrossRef](#)] [[PubMed](#)]
157. Ahn, S.; Lee, S.J. Nanoparticle role on the repeatability of stimuli-responsive nanocomposites. *Sci. Rep.* **2014**, *4*, 6624. [[CrossRef](#)] [[PubMed](#)]
158. Mondal, S. Stimuli responsive surfaces for fouling-resistant polymeric membranes. *J. Membr. Sci. Technol.* **2014**, *4*, 1. [[CrossRef](#)]
159. Clodt, J.I.; Filiz, V.; Rangou, S.; Buhr, K.; Abetz, C.; Höche, D.; Hahn, J.; Jung, A.; Abetz, V. Double stimuli-responsive isoporous membranes via post-modification of pH-sensitive self-assembled diblock copolymer membranes. *Adv. Funct. Mater.* **2013**, *23*, 731–738. [[CrossRef](#)]

